Accepted Manuscript

Early Paleoproterozoic magmatism in the Yangtze Block: Evidence from zircon U-Pb ages, Sr-Nd-Hf isotopes and geochemistry of ca. 2.3 Ga and 2.1 Ga granitic rocks in the Phan Si Pan Complex, north Vietnam

Tianyu Zhao, Peter A. Cawood, Jian-Wei Zi, Kai Wang, Qinglai Feng, Quyen Minh Nguyen, Dung My Tran

PII: S0301-9268(18)30604-1
DOI: https://doi.org/10.1016/j.precamres.2019.01.012
Reference: PRECAM 5263

To appear in: *Precambrian Research*

Received Date: 21 November 2018
Revised Date: 23 January 2019
Accepted Date: 24 January 2019

Please cite this article as: T. Zhao, P.A. Cawood, J-W. Zi, K. Wang, Q. Feng, Q.M. Nguyen, D.M. Tran, Early Paleoproterozoic magmatism in the Yangtze Block: Evidence from zircon U-Pb ages, Sr-Nd-Hf isotopes and geochemistry of ca. 2.3 Ga and 2.1 Ga granitic rocks in the Phan Si Pan Complex, north Vietnam, *Precambrian Research* (2019), doi: https://doi.org/10.1016/j.precamres.2019.01.012

Early Paleoproterozoic magmatism in the Yangtze Block: Evidence from zircon U-Pb ages, Sr-Nd-Hf isotopes and geochemistry of ca. 2.3 Ga and 2.1 Ga granitic rocks in the Phan Si Pan Complex, north Vietnam

Tianyu Zhao [a, b], Peter A. Cawood [b, c], Jian-Wei Zi [a, d], Kai Wang [e], Qinglai Feng [a *], Quyen Minh Nguyen [a, f], Dung My Tran [g]

[a] *State Key Laboratory of Geological Processes and Mineral Resources, China University of Geosciences, Wuhan, 430074, China*
[b] *School of Earth, Atmosphere & Environment, Monash University, Melbourne, VIC 3800, Australia*
[c] *Department of Earth Sciences, University of St. Andrews, North Street, St. Andrews KY16 9AL, UK*
[d] *John de Laeter Centre, Curtin University, Perth 6102, Australia*
[e] *Chinese Academy of Geological Sciences, Beijing 100037, China*
[f] *Department of Geology, Hanoi University of Mining and Geology, Hanoi, Viet Nam*
[g] *General Department of Geology and Minerals of Viet Nam, Hanoi, Vietnam.*

Corresponding author: qinglaifeng@cug.edu.cn (QLF)

Abstract

Our understanding of the early evolution of the Yangtze Block is limited by the sparsely dispersed nature of pre-Neoproterozoic exposures. New, integrated petrographic, zircon U-Pb age and Hf-Nd isotope analyses, and whole-rock geochemical data for early Paleoproterozoic granites in the Phan Si Pan Complex provides new insights into the evolution of the Yangtze Block as well as its role in the Pre-Nuna supercontinent. LA-ICP-MS zircon U-Pb dating of magmatic zircons from quartz monzonite and gneissic granite yielded $^{207}Pb/^{206}Pb$ ages of 2306 ± 12 Ma and 2096 ± 15 Ma, respectively. Zircons from the quartz monzonite have $\varepsilon_{Hf(t)}$ values ranging from -4.1 to -2.1, corresponding to T_{DM2} model ages of 3002–2890 Ma, whereas zircons in the gneissic granite have $\varepsilon_{Hf(t)}$ values between -0.95 and +1.72 and corresponding T_{DM2} model ages of 2660–2516 Ma, which are consistent with their whole-rock Nd isotope values. Geochemically, the quartz monzonites are I-type granites. Combined with their relatively high Sr/Y ratios and low Y concentrations, as well as fractionated REE patterns with relatively high LREE but low HREE concentrations, they were probably generated by partial melting of the thickened middle-lower crust under elevated temperature. Geochemical and isotopic signatures suggest that the ca. 2.1 Ga gneissic granites are high-K calc-alkaline, ferroan A-type granites formed by partial melting of juvenile crustal source at high temperature and low pressure with little involvement of ancient crustal material. The Phan Si Pan complex has a distinct early Paleoproterozoic crustal evolution history compared with the other crustal provinces of the Yangtze Block, suggesting independent histories that were not unified until the late Paleoproterozoic during the assembly of Nuna. Moreover, the magmatism and tectonic evolution of the north Vietnam region is broadly similar to that of the Arrowsmith Orogen of the Rae craton in Laurentia suggesting a potential spatial linkage. The geologic record of the Yangtze Block does not support an early Paleoproterozoic shutdown of plate tectonics.

Keyword: Zircon U-Pb-Hf isotopes; Geochemistry; Early Paleoproterozoic; Yangtze Block; Nuna supercontinent

1. Introduction

The Paleoproterozoic Era corresponds with changing thermal and tectonic regimes on Earth (Laurent et al., 2014), and the formation of the first true supercontinent, Nuna (also known as Columbia, e.g., Rogers and Santosh, 2002; Zhao et al., 2002). Middle to late Paleoproterozoic (2.1–1.8 Ga) magmatism and metamorphism associated with the assembly of Nuna has been documented across many of the major continental blocks (Zhao et al., 2002; Evans et al., 2016). In contrast, the magmatic record of the early Paleoproterozoic (2.5–2.1 Ga) is limited and is suggested by some to represent a global magmatic slowdown, also referred to as the Siderian Quiet Interval (e.g., Condie et al., 2009; Spencer et al., 2018).

However, early Paleoproterozoic magmatic rocks, although not voluminous, have been documented from Canada, South America, Africa, Europe, China and India (Partin et al., 2014, and references therein). This led Partin et al. (2014) to argue that convergent plate tectonics and juvenile crustal production was active during the period of the proposed magmatic and tectonic shutdown, and that a lack of zircons of this age might be an artifact of preservation or a bias in sampled localities.

The early Paleoproterozoic crustal history of the Yangtze Block has been largely limited to detrital zircon ages (2.3–2.1 Ga; Greentree and Li, 2008; Hieu et al., 2012) and a few rock outcrops (2.30–2.29 Ga; ignimbrite, Zhu et al., 2011; Zhou et al., 2012) in the western Yangtze Block, but available robust ages and geochemistry constraints are still lack for establishing an early Paleoproterozoic crustal evolution of the block and its position prior to the final assembly of the Nuna supercontinent. The history of the Yangtze Block of the South China Craton commenced some 3.45 billion years ago (Guo et al., 2014), and involved sporadic Archean granitic magmatism among different crustal provinces (i.e. the Kongling Complex, the Zhongxiang Complex and the Yudongzi Complex), widespread late Paleoproterozoic magmatism and metamorphism (2.05–1.75 Ga; Wang et al. 2018a, b and references therein), and Neoproterozic orogenic-related magmatism (e.g., Zhao et al., 2018). However, the recently discovered Phan Si Pan Complex in north Vietnam is regarded as the southern continuation of the Yangtze Block (Lan et al., 2001; Nam et al., 2003). Age determinations on orthogneisses of this complex reveal episodes of Paleoproterozoic magmatism (i.e., 2.28–2.19 Ga and 1.85 Ga; Nam et a., 2003; Wang et al., 2016). As yet, the rock associations and the precise timing and origin of the Phan Si Pan Complex are not fully understood, and their implications for the early formation and evolutionary process of the Yangtze Block are equivocal. In this paper, we present new zircon U-Pb age and Lu-Hf isotopes, as well as whole-rock major, trace element, and Sr-Nd isotopes results from the early Paleoproterozoic granitoids in north Vietnam. The data allows us to characterize the petrogenesis and geological setting of the magmatic activity, which in combination with the regional geologic record in the Yangtze Block, enable us to provide an updated interpretation of Paleoproterozoic crustal evolution of the Yangtze Block and its position prior to final assembly of the Nuna supercontinent. Furthermore, our results suggest that plate tectonics did not shut down during early Paleoproterozoic between 2.45 and 2.2 Ga.

2 Geologic background

The South China Craton is bounded by the Qinling-Dabie orogenic belt to the north, the Longmenshan Fault on the west, and the Ailaoshan-Song Ma Suture Zone to the south (Fig. 1). It is composed of the Yangtze and Cathaysia blocks, separated by the Neoproterozoic Sibao (Jiangnan) Orogen (Fig. 1; Cawood et al., 2018). The Yangtze Block, dominated by Neoproterozoic and Phanerozoic sequences and igneous rocks, exposes the oldest crystalline rocks of the South China Craton, including 3.45–2.62 Ga metamorphosed granites (TTGs) and mafic rocks of the Kongling Complex, 2.90–2.62 Ga granitic rocks, and 2.70–2.67 Ga supracrustal rocks of the Zhongxiang Complex. Middle to late Paleoproterozoic granitic plutons (2.0–1.70 Ga) intruded most of the Archean crustal provinces in the Yangtze Block, but early Paleoproterozoic rocks are only documented in the Dongchuan region of the southwestern Yangtze Block (Tangdan Group ignimbrite, 2.30 Ga; Zhu et al., 2011) and north Vietnam (2.28–2.19 Ga orthogneisses; Wang et al., 2016). The Dongchuan region also preserves the only late Paleoproterozoic to earliest Mesoproterozoic (1.8–1.5 Ga) volcanic-sedimentary successions of the Yangtze Block, which were intruded by coeval granites and mafic rocks (e.g., Zhao et al., 2010; Chen et al., 2013; Kou et al., 2017).

The Yangtze Block extends into north Vietnam as far south as the Song Ma Suture Zone, where it is generally divided into the NW and NE parts by the Cenozoic Ailaoshan-Red River shear zone (Figs. 1 and 2; Rossignol et al., 2018). Precambrian rocks in north Vietnam mainly crop out in the Phan Si Pan Complex and the Neoproterozoic Nam Co unit (Fig. 2). The Phan Si Pan Complex is exposed as a narrow belt along the southwest side of the Ailao Shan-Red River shear Fault. The Phan Si Pan Complex is composed of Archean and Paleoproterozoic rocks, which were metamorphosed to greenschist and amphibolite facies, and are unconformably overlain by Paleozoic strata (Wang et al., 2016). Geochronological studies reveal that the Phan Si Pan Complex includes 2.90–2.84 Ga TTG gneiss (Lan et al., 2001; Nam et al., 2003), 2.28–2.19 Ga granitic gneiss (Wang et al., 2016), 1.85 Ga granitoids (Anh et al., 2015), and the Paleoproterozoic Sinh Quyen sedimentary sequences (Hieu et al., 2012). These Archean-Paleoproterozoic rocks are intruded by several Neoproterozoic plutons (824–736 Ma; Li et al., 2018). The Neoproterozoic Nam Co Unit, on the south-side of Phan Si Pan Complex, comprises mainly greenschist, mica–quartz schist, quartzite and phyllite (Zhang et al., 2013). The Cenozoic Day Nui Con Voi massif, a large-scale antiformal 'core complex'-type structure, bounded by the Ailaoshan-Red River shear zone and the Song Chay fault, records deformation along the Red River zone in north Vietnam (Hieu et al., 2016). The Song Ma Suture Zone has been regarded as a major suture zone with relics of oceanic lithosphere, including ophiolite, metabasite, metasedimentary rocks and eclogite (Zhang et al., 2013). The NW–SE directed Song Da–Tu Le intracontinental rift system is located between the Phan Si Pan Complex in the northeast and the Nam Co Unit in the southwest. The Song Da rift mainly contains Devonian to Middle Triassic sedimentary-volcanic sequences. The Tu Le basin contains Late Permian acidic to intermediate magmatic rocks, including rhyolite, trachyrhyolite and trachydacite.

3 Sampling and analytical methods

In this study, two samples, one quartz monzonite (16vn02-09) and one gneissic granite (16vn02-06) collected from Phan Si Pan Complex were used for zircon U-Pb dating and Lu-

Hf isotopic analysis. An additional 15 samples (6 quartz monzonites and 9 gneissic granites) were collected close to each geochronological sample for whole-rock geochemical analysis. The quartz monzonites were taken from outcrops at 21°08′41.75″ N, 105°00′55.82″ E and the gneissic granites were taken at 21°02′38.50″ N, 105°01′36.52″ E. The newly identified quartz monzogranites and gneissic granites were emplaced into the southwestern part of the Phan Si Pan Complex (Fig. 2 and 3A, B). The quartz monzogranite comprises K-feldspar, plagioclase, quartz, biotite and muscovite, with accessory minerals zircon, titanite, and opaque oxide minerals (Fig. 3C and D). Muscovite is not primary but the result of alteration of biotite and feldspar. The gneissic granite is mainly composed of K–feldspar, quartz, plagioclase, and biotite (Fig. 3E and F), with accessory minerals including zircon and opaque oxides. They have gneissic fabrics defined by aligned quartz and biotite.

3.1 Zircon U–Pb dating

Zircon grains from the samples were separated by conventional magnetic and density separation procedures and were then picked by hand under a binocular microscope. About 200 grains were randomly selected from each individual sample, mounted in epoxy and polished to expose the center of the crystals. Cathodoluminescence (CL) images were obtained using a JEOL JXA-8100 electron microscope to reveal the morphologies and internal structures of the zircon grains. Zircon U–Pb dating was carried out at the State Key Laboratory of Geological Processes and Mineral Resources, China University of Geosciences, Wuhan using an Agilent 7500a ICP-MS equipped with a 193 nm Geolas 2005M laser–ablation system. Detailed analytical procedure followed Liu et al. (2010). For each analysis, we used a spot diameter of 32 μm with 20 s gas blank and 50 s signal acquisition. Zircon standards 91500 and GJ–1 were used to calibrate U/Pb ratios and to monitor isotope fractionation, respectively. The standard 91500 was analyzed twice every 8 analyses. NIST 610 glass was analyzed to correct the time-dependent drift of sensitivity and mass discrimination for the trace element analysis. Off-line selection and integration of background and analytical signals, time-drift correction and quantitative calibration for the raw U–Pb dating were performed using ICPMSDataCal (Liu et al., 2008). Common Pb-corrected U-Pb ages and concordia diagrams were prepared using Isoplot/Ex_ver3 (Ludwig, 2003).

3.2. Zircon Hf isotopic analysis

In situ zircon Lu–Hf isotopic analysis was undertaken on dated zircon grains using a Neptune Plus MC-ICP-MS in combination with a Geolas 2005 excimer ArF laser ablation system at the State Key Laboratory of Geological Processes and Mineral Resources, China University of Geosciences, Wuhan. Detailed instrument settings and analytical method were similar to those described by Hu et al. (2012). We employed a spot diameter of 44 μm and 20 s background signal followed by 50 s of ablation signal acquisition. The standard 91500 was analyzed twice every 9 analyses. The $^{179}Hf/^{177}Hf$ and $^{173}Yb/^{171}Yb$ ratios were used to calculate the mass bias of Hf (β_{Hf}) and Yb (β_{Yb}), which were normalized to $^{179}Hf/^{177}Hf$ = 0.7325 and $^{173}Yb/^{171}Yb$ = 1.1248 (Blichert-Toft et al., 1997) using an exponential correction for mass bias. The interference of ^{176}Yb on ^{176}Hf was corrected by the recommended $^{176}Yb/^{173}Yb$ ratio of 0.7876 (McCulloch et al., 1977) to calculate $^{176}Yb/^{177}Hf$. The minor interference of ^{176}Lu on ^{176}Hf was corrected by $^{176}Lu/^{175}Lu$ = 0.02656 (Blichert-Toft et al., 1997) to calculate $^{176}Lu/^{177}Hf$. The values of initial Hf isotope and $^{176}Hf/^{177}Hf$ ratios were calculated employing the ^{176}Lu decay constant of $1.865 \times 10^{-11} a^{-1}$ (Scherer et al., 2001) and the measured $^{176}Lu/^{177}Hf$ ratios. The Hf model ages (T_{DM1}) were calculated based on the depleted mantle model, and two-stage Hf model ages (T_{DM2}) were calculated by assuming a $^{176}Lu/^{177}Hf$ ratio of 0.015 for the average continental crust (Griffin et al., 2006).

3.3 Whole-rock geochemical analysis

Samples were crushed and powdered in a WC mill to approximately 200 mesh. Major elements were analyzed by X-ray fluorescence (XRF) spectrometry at the State Key Laboratory of Geological Processes and Mineral Resources, China University of Geosciences, Wuhan. 0.5 g of rock powder and 5 g of compound flux ($Li_2B_4O_7$:$LiBO_2$ = 12:22) were heated at ~1050°C in a Pt crucible for 11 minutes to make fused glass disks and were later measured on an XRF–1800. The loss-on-ignition (LOI) was measured by recording the percentage weight loss on dried rock powder by heating in a pre-heated corundum crucible to 1000°C for two hours. Trace element analyses were conducted on an Agilent 7700e ICP-MS at the GPMR, CUGW. The analytical precision is better than 5 % for elements with abundances >10 ppm, better than 8 % for those with abundances <10 ppm, and 10 % for transition metals.

The Sr and Nd isotopic compositions were determined in static mode on the Nu Plasma MC-ICP-MS. Approximately 100 mg whole-rock powders were digested in sealed Teflon bombs with a mixture of concentrated HNO_3, HF and $HClO_4$. The sealed bombs were kept in an oven at 190°C for 48 h. The decomposed samples were then dried at 140°C followed by adding concentrated HNO_3 and HCl. Sr and Nd (and other REEs) were separated/concentrated using standard chromatographic columns with AG50W-X8 and HDEHP resins following the procedure of Gao et al. (2004). The measured $^{143}Nd/^{144}Nd$ and $^{87}Sr/^{86}Sr$ ratios were normalized to $^{146}Nd/^{144}Nd$ = 0.7219 and $^{86}Sr/^{88}Sr$ = 0.1194, respectively.

4. Analytical Results

4.1. Zircon U-Pb geochronology and Lu-Hf isotopes

Zircons from sample 16VN02-09 (quartz monzonite) are mainly transparent, light brown and prismatic (80–400 μm), with aspect ratios between 2:1 and 4:1 (Fig. 4A). In CL images, all the zircons show oscillatory zoning and a few zircon grains display core-rim microstructures. The luminous rims possibly indicate that they have experienced variable degrees of modification related to metamorphic fluid/melt, however they are too thin to analyzed. U and Th contents of the analyzed zircons range between 186 and 851 ppm and between 71 and 208 ppm, respectively, with Th/U ratios of 0.19 to 0.53. Twenty-four analyses together yielded a mean $^{207}Pb/^{206}Pb$ age of 2306 ± 12 Ma (MSWD = 0.69; Fig. 5A; Appendix Table S1), which is interpreted as the igneous crystallization age of the quartz monzonite.

Zircons crystals from the sample 16VN02-06 (gneissic granite) are colorless to pale brown, and euhedral (100–400 μm long) with aspect ratios of 1:1–4:1 (Fig. 4B). They typically show concentric oscillatory zoning in CL images. The zircons have Th and U concentrations varying from 38 to 734 ppm and 61 to 1066 ppm, respectively, with Th/U ratios from 0.33 to 0.76. Seventeen analyzed zircon crystals from the sample 16VN02-06 gave a weighted mean $^{207}Pb/^{206}Pb$ age of 2096 ± 15 Ma (MSWD = 0.79; Fig. 5B; Appendix Table S1), which is interpreted as the igneous crystallization age of the granite protolith.

Twelve analyses on zircons from sample 16VN02-09 gave $^{176}Hf/^{177}Hf$ ratios of 0.281224–0.281281, corresponding to $\varepsilon_{Hf(t)}$ of -4.18 to -2.09 (Fig. 6) and Hf crustal model ages (T_{DM2}) of 3002–2890 Ma (Appendix Table S2). Thirteen analyses obtained from sample 16VN02-06 yielded $^{176}Hf/^{177}Hf$ ratios of 0.281465–0.281559, corresponding to $\varepsilon_{Hf(t)}$ of -0.95 to 1.72 and Hf crustal model ages (T_{DM2}) of 2660–2516 Ma (Fig. 6 and Appendix Table S2).

4.2 Whole-rock major and trace element geochemistry

The gneissic granites (16VN02-06) have very low LOI (0.32–0.68 wt. %, lower than 1 wt. %) suggest that the rocks have not been subjected to any major alteration. Therefore, whole-rock geochemical analyses were carried out to better understand their rock types and magma sources. However, the quartz monzonite (16VN02-09) have variable LOI (1.08–3.16 wt. %) suggest that the rocks have been subjected to minor amount of alteration. Therefore, an assessment of the element mobility prior to a discussion of their petrogenesis (quartz monzonite) is necessary and only the immobile elements can be used for interpretation of the petrogenesis. A number of elements (K_2O, CaO, MgO, P_2O_5, FeOT, Y, Rb, La, Yb, Sr, Ti and Nb) with different geochemical behaviors were plotted against Zr (Fig. S1 A-K), which is generally used as an alteration-independent index during low-grade metamorphism and hydrothermal alteration (Polat and Hofman, 2003). As shown in Fig. S1, the high-field-strength elements (HFSEs; e.g., Y, La, Yb, Ti and Nb) and some major elements (e.g., MgO, P_2O_5 and FeOt) have good correlations with Zr, indicating these elements are essentially immobile and preserve the original signatures. On the contrary, most large-ion-lithophile elements (LILEs; e.g., K, Rb and Ca), except for Sr, are scattered for the samples, suggesting varying degrees of mobility during metamorphism and alteration. In addition, sample 16vn02-09-2 has the lowest LOI, suggesting its composition closely reflects the primary magmatic signatures of the rocks. Thus, only those immobile elements and relatively fresh samples were used in the following discussion.

Major and trace element data for the samples are listed in Appendix Table S3. The 2306 Ma quartz monzonites show variable major element compositions (SiO_2 = 65–71 wt. %, Al_2O_3 = 13.78–17.86 wt. %, CaO = 0.84–1.52 wt. %, and P_2O_5 = 0.1–0.19 wt. %). They contain high alkali (K_2O = 3.16–4.00 wt. %; Na_2O = 3.78–4.85 wt. %) and low MgO (0.55–1.08 wt. %) and Fe_2O_3T (2.59–3.61 wt. %) contents. Their Mg# (Mg# = Mg / (Mg + Fe) × 100) range from 32 to 46. In the plot of Nb/Y vs. Zr/TiO_2 (Fig. 7A), they fall into the monzonite field. They belong to high-K calc-alkaline and magnesian series (Fig. 7B and C). They are weakly to strongly peraluminous with A/CNK values of 1.02 to 1.44. They have pronounced negative Nb and P anomalies on the spider diagram (Fig. 8A). They are characterized by high Sr/Y ratios of 18–44. All the samples show LREE-enriched and HREE-depleted patterns (Fig. 8B) with high $(La/Yb)_N$ values (49.6–141) and weakly negative to positive Eu anomalies (δEu = 0.69–1.32, where $\delta Eu = Eu/\sqrt{(Sm*Gd)}$). Whole-rock Zr saturation temperatures (Watso and Harrision, 1983) of the quartz monzonites gave T_{Zr} values from 815 to 863°C.

In contrast, the 2096 Ma gneissic granites exhibit restricted and high SiO_2 (75–77 wt. %), K_2O (5.00–5.83 wt. %), but low CaO (0.24–0.36 wt. %) and Mg# (10–16). In the plot of Nb/Y vs. Zr/TiO_2 (Fig. 7A), they fall into the fields of granite. They are high-K calc-alkaline, ferroan and mostly slightly peraluminous (i.e. A/CNK = 1.04–1.10, except for the one sample with A/CNK of 1.13; Fig. 7B-D). In the primitive mantle-normalized spider diagram, the samples display significant depletion of Ba, Nb, Sr, P and Ti and enrichment of U, Nd and Zr (Fig. 8C). Compared to the 2306 Ma quartz monzonites, they have higher total REE abundances of 481–698 ppm (Fig. 8D and Appendix Table S3) with moderate enrichment in the light rare earth elements (LREE, $(La/Yb)_N$ = 10.14–20.75), little fractionation in the heavy rare earth elements (HREE) and distinct negative Eu anomalies (δEu = 0.18–0.29). Whole-rock Zr saturation temperatures of the gneissic granites gave T_{Zr} values from 872 to 898 °C.

4.3 Whole-rock Sr-Nd isotopic compositions

Three samples from the quartz monzonites and three samples from the gneissic granite were analyzed for their Sr and Nd isotopic compositions, which are presented in Appendix Table S4.

The quartz monzonites yielded $^{87}Sr/^{86}Sr$ ratios of 0.756633–0.766243, with the calculated initial $^{87}Sr/^{86}Sr$ (t) ratios of 0.702496 to 0.712289. The measured $^{143}Nd/^{144}Nd$ ratios are between 0.510704 and 0.511033, and the calculated $\varepsilon_{Nd(t)}$ values vary from −3.34 to −2.75, and the two-stage Nd model ages vary from 3.01 to 2.96 Ga.

The gneissic granites have high $^{87}Rb/^{86}Sr$ ratios that result in inaccurate initial $^{87}Sr/^{86}Sr$ ratios (0.572530–0.633105). The large variation of the initial Sr isotope ratios might result from disturbances of the Rb–Sr isotope system by subsequent metamorphism (Wu et al., 2012). The REEs, including Sm and Nd, are considered to be much less mobile than Rb and Sr during metamorphism and hydrothermal processes. The Sm–Nd isotopic system is usually robust, and is thus considered to closely reflect the primary magmatic signatures of the rocks (Wu et la., 2002). They have measured $^{143}Nd/^{144}Nd$ values of 0.509917 to 0.510001with $\varepsilon_{Nd(t)}$ values varying from −0.11 to 1.54, and the two-stage Nd model ages varying from 2.57 to 2.43 Ga.

5. Discussion

5.1 Petrogenesis of 2.30 Ga quartz monzonites

5.1.1 Genetic types and magma source

Granites are generally grouped into I-, S-, A- and M-types according to magma sources and generation mechanisms (Collins et al., 1982; Whalen et al., 1987; Eby, 1992; Chappell, 1999). The circa 2.30 Ga quartz monzonites have magnesian compositions and are distinguished from typical A-type granite by low Ga/Al ratios (Fig. 9A-D). They are strongly peraluminous, a characteristic of S-type granites derived from partial melting of metasedimentary rocks. However, there is a direct correlation between A/CNK values and LOI values in these samples (Fig. S1L). The sample of 16vn02-09-2 with lowest LOI have low A/CNK of 1.08, which is analogous to I-type granites (A/CNK <1.1; e.g., Chappell et al., 1999, 2012). The high A/CNK of samples could be the leaching out of K and Ca by alteration, because these elements tend to be mobile. Moreover, the 2.3 Ga quartz monzonite lack typical peraluminous minerals such as cordierite and garnet, while some muscovite formed from the alteration of igneous biotite and feldspar. No inherited zircon cores were observed in the CL images. These observations suggest that metasedimentary rocks are not the likely source of the 2.30 Ga quartz monzonites. Experimental petrology studies reveal that partial melting of metaluminous mafic to intermediate rocks at mid-to-lower crustal pressures can also produce peraluminous melts (e.g., Patiño Douce and Beard, 1995; Sisson et al., 2005). According to the experimental results, the quartz monzonites were mostly likely formed by partial melting of mafic to intermediate igneous sources. The analyzed samples display a negative correlation between P_2O_5 and SiO_2 (Fig. 10A), which are features typical of I-type granite (Chappell et al., 1998, 1999, 2012; Chappell and White, 1992; Clemens, 2003). Additionally, the high zircon saturation temperatures for the samples (826–863^oC) are in contrast with normal S-type granites, which are characterized by low temperatures (<800 ^oC; Chappell et al., 2004). Thus, the 2.30 Ga quartz monzonites are classified as I-type granites.

The 2.30 Ga quartz monzonites show moderate Mg# values (32.6–46.2), depletions in HFSE (e.g., Nb and Ti), enrichment in Rb and K, together with a restricted range of negative $\varepsilon_{Hf}(t)$ (-2.1 to -4.1) and $\varepsilon_{Nd(t)}$ (−3.38 to −2.79), suggesting they were derived from a relatively homogenous crustal protolith with possible limited mantle materials. The narrow range of $\varepsilon_{Hf}(t)$ and $\varepsilon_{Nd(t)}$ are also atypical for S-type granites corresponding to T_{DM2} (2.9–3.0 Ga) of $\varepsilon_{Hf(t)}$ and $\varepsilon_{Nd(t)}$ values, which generally show a wide range of values.

5.1.2 Melting conditions

The 2.30 Ga quartz monzonites have fractionated REE patterns with high $(La/Yb)_N$ (49–141) and generally slightly positive Eu anomalies, associated with high Sr/Y values. Combined with their high Sr/Y and high $(La/Yb)_N$ ratios (Fig. 11), we suggest that the magma source was within the stability field of garnet and/or amphibole without plagioclase. These features are similar to adakites generated in a relatively high pressure (Fig. 11; Martin et al., 2005). However, compared to typical adakites, the 2.30 Ga quartz monzonites yield lower Sr concentrations (<400 ppm) and flat HREE patterns. The quartz monzonites have flat HREE patterns, which suggest that amphibole rather than garnet played a more important role during partial melting. This indicates that garnet-bearing amphibolite rather than eclogite is the main residual phase (Gromet and Silver, 1987).

High Sr/Y and $(La/Yb)_N$ ratios are commonly attributed to high-pressure magmatic processes, such as partial melting of subducted juvenile oceanic crust, metasomatized lithospheric mantle, or partial melting of a thickened lower crust (Martin et al., 2005; Rollinson and Martin, 2005; Zhao et al., 2017). However, the low Mg#, Cr, and Ni values and negative $\varepsilon_{Hf(t)}$ and $\varepsilon_{Nd(t)}$ values preclude these rocks being derived from subducted juvenile oceanic crust or metasomatized lithospheric mantle. This is because interactions with peridotitic mantle during magma ascent would result in high Mg#, Cr and Ni and depleted $\varepsilon_{Hf(t)}$ and $\varepsilon_{Nd(t)}$ values (Martin et al., 2005; Nagel et al., 2012). Experimental petrology studies have shown that partial melting of mafic lower crust would produce low Mg number melts (<45; Rapp and Watson, 1995). The low Mg numbers (32–46) and MgO (0.55–1.08 wt. %), suggests the 2.30 Ga quartz monzonites originated in the middle to lower crust. Therefore, the ca. 2.30 Ga quartz monzonites are interpreted to originate from the partial melting of over-thickened crust (Atherton and Petford, 1993; Rapp and Watson, 1995). Moreover, the calculated T_{Zr} = 826–863 °C of the samples suggest that they are “hot granites” (Miller et al., 2003).

The relatively high-T and high-P conditions for formation of the 2.30 Ga quartz monzonites are similar to granite formed by crustal thickening in zones of collisional orogenesis (Pearce et al., 1984; Barbarin, 1996, 1999; Chen et al., 2017). The most effective thickening process would be tectonic shortening due to the convergence of plates, such as arc-continent or continent-continent collision (Hsu and Sibuet, 1995; Giese et al., 1999). In the Ta versus Yb discrimination diagram, the 2.30 Ga samples plot in the syn-collision granite field (Fig 13). In addition, 2.36 Ga high-grade tectono-metamorphic events are recorded by the ca. 2.9 Ga orthogneissic rocks in the Phan Si Pan complex of north

Vietnam (Nam et al., 2003). Therefore, the 2.30 Ga quartz monzonites in the Phan Si Pan Complex are interpreted to be the partial melts of previously thickened and thermally equilibrated basaltic to intermediate middle-lower crust resulting from collisional orogenesis (e.g., Huang et al., 2013).

5.2 Petrogenesis of ca. 2.1 Ga gneissic granite

5.2.1 Genetic types

The 2.10 Ga gneissic granites have high SiO_2 contents, $(K_2O+Na_2O)/CaO$, Ga/Al and Fe/Mg ratios, enrichment in HFSE (e.g., Zr, Nb, and Y) and REE (except for Eu), and low Cao, MgO, Cr, Ni, Eu, Sr and Ba. They are geochemically distinct from the 2.30 Ga quartz monzonites but similar to typical A-type granites (Whalen et al., 1987; Creaser et al., 1991; Eby, 1992; King et al., 1997). On the other hand, the 2.10 Ga gneissic granites show high-K calc-alkaline, weakly peraluminous features (with A/CNK ratios of 1.04–1.13), similar to ferroan granites (Fig. 7C; Frost et al., 2001). All the samples plot within the A-type granite fields on major and trace elements discrimination diagrams (Fig. 9A-D; Whalen et al., 1987). However, highly differentiated S- and I-type granites can also show A-type granitic characteristics (Whalen et al., 1987; King et al., 1997; Wu, 2007). A highly differentiated origin for the 2.10 Ga gneissic granites can be excluded for the following reasons: (1) they have high FeOT (1.8–2.3 wt. %) and FeOT/MgO (2.44–4.34) in contrast to highly fractionated I-type and S-type granites (Whalen et al., 1987; Eby, 1992); (2) they have high Zr + Nb + Y + Ce (298–491 ppm), which is different from fractionated I-, S- and M-type granitoids with low Zr + Nb + Ce + Y, because fractionation processes would reduce the HSFE contents in the magma (Whalen et al., 1987); (3) they have higher crystallization temperatures (calculated T_{Zr} range from 872 to 898 ^{o}C) than peraluminous I- and S-type granites, which further supports the A-type signature (King et al., 1997; Chappell et al., 2004; Bonin, 2007; Zhao et al., 2008b).

5.2.2 Magma sources of 2.1 Ga A-type gneissic granites

A-type granites can be produced by: (1) fractional crystallization of mantle-derived mafic magma with or without assimilation of crustal rocks (Turner et al., 1992; Eby, 1992; Mushkin et al., 2003; Bonin, 2007); (2) partial melting of a crustal source, either continental crust or earlier underplated mafic magmas (Collins et al., 1982; Creaser et al., 1991; Patiño Douce, 1997; Wu et al., 2002; Frost and Frost, 2011; Huang et al., 2011); (3) mixing of mantle-derived and crustal end-members coupled with later fractional crystallization (Bédard, 1990; Anderson et al., 2003; Yang et al., 2006).

The 2.10 Ga gneissic granites have similar $\varepsilon_{Hf(t)}$ with the 2.1 Ga Huangling andesites in the Kongling Complex, northern Yangtze Block (Fig. 6), suggesting a similar source. The Huangling intermediate rocks are inferred to have been derived from partial melting of sub-arc lithospheric mantle above a subducting oceanic slab (Han et al., 2018). However, A-type granite differentiated from mantle-derived melts should have peralkaline compositions whereas the 2.10 Ga A-type gneissic granites have a weakly peraluminous character (Eby, 1992; King et al., 1997). Additionally, the 2.10 Ga A-type gneissic granites have high SiO_2 (>75 wt. %), and lower MgO, Cr and Ni concentrations, which rules out the possibility of fractional crystallization from coeval lithospheric mantle above a subducting oceanic slab. A magma mixing petrogenetic model can be excluded on the basis that the 2.10 Ga A-type gneissic granites lack cognate mafic enclaves and have a restricted range of isotopic values. The high silica abundance, high-K, calcic-alkalic, weak peraluminous features, and strong negative Eu anomalies suggest that the gneissic granites are primarily crust-derived. The zircon $\varepsilon_{Hf(t)}$ values of the 2.10 Ga gneissic granites straddle the chondritic line, indicating that the source region of the 2.10 Ga gneissic granites is mainly composed of juvenile crust material, whereas their zircon Hf model ages (T_{DM2}) are 2.6–2.5 Ga, older than their crystallization age, which suggest that extraction of juvenile crust from depleted mantle occurred in the late Neoarchean. In addition, some zircons have slightly negative $\varepsilon_{Hf(t)}$ values and sample 16vn02-06-2 also has negative $\varepsilon_{Nd(t)}$ (-0.17), suggesting little involvement of ancient crustal material. Accordingly, the ca. 2.10 Ga gneissic granites were likely to be derived from partial melting of pre-existing juvenile crustal materials.

5.2.3 Melting conditions

The 2.10 Ga gneissic granites are enriched in LREE and have flat HREE profiles (Fig. 8D), with marked negative Eu anomalies (Eu/Eu* = 0.19–0.29) and high Yb (4.7–8.1) and Y (46–88 ppm) and low $(La/Yb)_N$ and Sr/Y ratios. This suggests that they formed at a relatively shallow crustal level with plagioclase, but negligible amphibole/or garnet, was present in the residue. Moreover, the high Zr saturation temperatures of the 2.10 Ga gneissic granites indicate a high-temperature origin (Appendix Table S3). A high-temperature and low-pressure origin for granite generation is often a feature of extensional settings (Ferreira et al., 2015).

A-type granite can be formed in various geodynamic settings ranging from within-plate to plate boundaries (Luo et al., 2018; Mukherjee et al., 2018; Wu et al., 2018). Eby (1992) subdivided A-type granites into A_1 and A_2 chemical subgroups. The 2.10 Ga gneissic granites plot in the A_2-type granites in Y/Nb vs. Ce/Nb and Nb-Y-Ce discrimination diagrams (Fig. 9E and F), which is consistent with a crustal origin formed at a post-collisional setting (Eby, 1992). In the Ta versus Yb tectonic discrimination diagram, they plot in the within-plate field (Fig. 12).

6. Tectonic implications

6.1 Paleoproterozoic evolution of north Vietnam

Our new data from the Phan Si Pan Complex provide evidence for 2.30 Ga and 2.10 Ga magmatism in the North Vietnamese segment of the southern Yangtze Block. These data, along with the previously reported 2.28–2.25 Ga and 2.19 Ga granitic magmatism, 2.36 Ga and 1.97 Ga metamorphism (Wang et al., 2016), and 1.85 S-type granitic magmatism (Anh et al., 2015) in the Phan Si Pan Complex, demonstrate prolonged tectonic evolution for the southern Yangtze Block during the Paleoproterozoic. Chemical data for the 2.28–2.19 Ga granitic gneisses are not available.

The distinctly different whole-rock geochemistry and zircon Hf isotopic signatures of the 2.30 Ga quartz monzonites and 2.10 Ga A-type gneissic granites suggest that these rocks originated from different sources and formed in contrasting tectonic settings. Partial melting of thickened middle-lower crust at elevated temperature is invoked to explain the genesis of the 2.30 Ga quartz monzonites, whereas 2.10 Ga gneiss granites were derived by high-temperature but low-pressure partial melting of Neoarchean juvenile crustal sources with limited involvement of ancient crustal materials. These features, together with the ~200 Ma age difference, suggest that the two granitic phases represent products of unrelated events. Therefore, we argue at least two discrete tectonic events affected the region during early Paleoproterozoic. Metamorphism and magmatism, dated at 1.97–1.85 Ga, were possibly products of an additional tectonic event (Wang et al., 2016).

6.2 Implications for early Paleoproterozoic evolution of the Yangtze Block and its possible correlations with other cratons

Detrital zircons from metasedimentary rocks in the Phan Si Pan Complex have an age spectrum that ranges from 2.4 to 2.1 Ga (Hieu et al., 2012). The $\varepsilon_{Hf(t)}$ values of the early Paleoproterozoic detrital zircons from the Phan Si Pan Complex are indistinguishable with those of the ca. 2.3 Ga and 2.1 Ga magmatic zircons analyzed in the present study. This suggests that the 2.3–2.1 Ga magmatism was likely widespread in or near the Phan Si Pan Complex, and that the granites we dated could be a potential source to the metasedimentary rocks.

The ca. 2.1 Ga granites in north Vietnam are different from contemporaneous granites in the northern Yangtze in petrogenesis and tectonic setting. The ca. 2.1 Ga magmatic rocks of the Houhe Complex and Huangling dome in the northern Yangtze Block show geochemical characteristics of an Andean-type convergent margin (Wu et al., 2012; Han et al., 2018), whereas the ca. 2.1 Ga granite in north Vietnam formed in an extensional environment. Therefore, we speculate that north Vietnam was possibly an independent terrane separated from other parts of the Yangtze Block during the early Paleoproterozoic. Such an interpretation is consistent with (1) distinct metamorphic and magmatic events occurring in different Archean-Paleoproterozoic basement units in the Yangtze Block (Fig. 13A-G); (2) the distinct detrital zircon age patterns in the eastern, northwestern and southern parts of Yangtze Block (Wu et al., 2012; Yang et al., 2018; Wang et al., 2018b); (3) deep seismic reflection profile across the Sichuan basin that reveals division of the mid-lower crust into eastern and western parts, and a buried N-S trending Paleoproterozoic orogen beneath the central Yangtze Block (Dong et al., 2015; Xiong et al., 2016); (4) a N-S striking Paleoproterozoic ophiolitic mélange belt in the central part of North Kongling Complex (Han et al., 2017). Previous studies have documented ubiquitous late Paleoproterozoic (2.1–1.85 Ga) tectono-thermal imprints across the entire Yangtze Block including the north Vietnam (Wu et al., 2008; Yin et al., 2013; Wang et al., 2015, 2018b; Zhou et al., 2017), suggesting that Yangtze formed a single coherent continental block by the late Paleoproterozoic.

The position of the Yangtze Block within the Nuna supercontinent has either been ignored due to a lack of data (Rogers and Santosh, 2002; Zhao et al., 2002) or placed in a range of positions including both within or along the margins of the supercontinent (Yin et al., 2013; Zhou et al., 2014; Wang et al., 2015, 2016). The presence of a 2.0–1.9 Ga orogenic belt in the northern Yangtze has been used to argue for a position between the southwest of Australian and South African cratons (Yin et al., 2013; Wang et al., 2015).

Alternatively, on the basis of similar age spectra of detrital zircons, ca. 1.7 Ga within-plate magmatism, and similar IOCG deposits, the Yangtze Block was considered to be linked with the North Australian Craton during the Paleoproterozoic (Zhou et al., 2014). However, the position of the Yangtze Block prior to the final assembly of the Nuna supercontinent has remained poorly constrained due to the sparse record of early Paleoproterozoic tectonothermal events. Recently, the Paleoproterozoic tectono-thermal record of the north Vietnamese region of the Yangtze was compared with the Rae craton of Laurentia (Wang et al., 2016).

Table 1 is a global compilation of composition, tectonic setting and isotopic information for well-dated ca. 2.3 Ga magmatism. Unsurprisingly, the global contemporary magmatic record reveals a range of tectonic settings and isotopic information.

In South America, a Palaeoproterozoic magmatic event at this time was reported during the Transamazonian Orogeny (for the Amazonian Craton) and the Minas accretionary orogeny (for the São Francisco Craton; Dos Santos et al., 2009; Macambira et al., 2009; Seixas et al., 2012; Teixeira et al., 2015). Much of the ca. 2.3 Ga isotopic records in the South America continent have positive values with limited negative values and are related to intra-oceanic island arc settings (Table 1). In a similar manner, the interpreted continental arc-related setting for ca. 2.3 Ga magmatism in the Lüliang Complex, Taihua Complex and Hengshan Terrain of the North China Craton is characterized by juvenile-like isotopic characteristics with little ‘‘crustal” isotopic signatures (Table 1; Kröner et al., 2005; Zhao et al., 2008a; Diwu et al., 2014; Santosh et al., 2015; Yuan et al., 2017). In the Tarim Craton, ca. 2.3 Ga magmatism from the Quanji massif is interpreted to have formed in a post-collisional extensional tectonic regime displaying a heterogeneous Nd-Hf isotopic compositions, while those from Heluositan Group are formed in continental rift with negative $\varepsilon_{Nd(t)}$ values (Zhang et al., 2007; Gong et al., 2014; He et al., 2018). The ca. 2.3 Ga mafic dykes from the Dharwar Craton of India, North Atlantic Craton, Karelian Craton and Fennoscandian Shield of Europe, and mafic-intermediate rocks from the Congo and Zimbabwe Cratons show variable isotopic compositions linked to LIP/rifting events, possibly associated with the breakup of late Archean cratons (Tchameni et al., 2001; Manyeruke et al., 2004; Kullerud et al., 2006; French and Heaman, 2010; Kumar et al., 2012; Nilsson et al., 2013; Stepanova et al., 2015).

A closer match to the early Paleoproterozoic tectonic evolution of north Vietnam may be provided by the Arrowsmith Orogen of the Rae Craton in Laurentia. There, a suite of 2.33–2.29 Ga syn- to post-collisional granites, and subsequent 2.19–2.02 Ga post-orogenic peralkaline intrusive complexes has been identified (Hartlaub et al., 2007). In north Vietnam, ca. 2.3 Ga syn-collisional I-type granites were followed by to post-orogenic extension and intrusion of A-type granites at ca. 2.1 Ga. Moreover, the 2.3 Ga granites in the Arrowsmith Orogen have Nd model ages (2.87–3.05) comparable to coeval granite Nd model ages (2.96 to 3.01 Ga) in north Vietnam. Additionally, the Arrowsmith orogen records ∼700°C and 0.5–0.6 GPa peak conditions of amphibolite- to granulite-facies metamorphism at 2.4–2.3 Ga (Berman et al., 2013). Similar metamorphic conditions (reached ∼700°C and 0.65 GPa) are also recorded in north Vietnam at ca. 2.36 Ga (Nam et al., 2003), suggesting possible involvement of the Yangtze Block in the Arrowsmith orogen (Wang et al., 2016). The similar tectonic framework of the two blocks supports a close spatial relationship during the early Paleoproterozoic (cf. Wang et al., 2016).

6.3 **No early Paleoproterozoic plate tectonic shutdown**

The early Paleoproterozoic Era, also referred to as the Siderian Quiet Interval (2.5–2.1 Ga), has been considered as a relatively quiescent geologic processes as tracked from a paucity of detrital sediments worldwide (Condie et al., 2009). As mentioned above, the available data show that ca. 2.5–2.2 Ga magmatism have been widely reported in the major cratons worldwide (Table 1). The prominent early Paleoproterozoic magmatic records and U–Pb detrital ages for Paleoproterozoic metasedimentary rocks in the Yangtze shield provide indirect evidence for a development of early Paleoproterozoic crust (Hieu et al., 2012 and this study). Thus, we suggest that the early Paleoproterozoic Era of a "global plate tectonic shutdown" is at the very least less global than previously suggested.

7. Conclusion

(1) Magmatic activity within the Phan Si Pan Complex of the southern Yangtze Block, north Vietnam, is dated at ca. 2.3 Ga and ca. 2.1 Ga.

(2) The 2.3 Ga quartz monazite was likely generated by partial melting of thickened middle-lower crust at high temperature, and followed a collision-related crustal thickening event.

(3) The 2.1 Ga A-type gneissic granite is the product of partial melting of a juvenile crustal source with minor involvement of ancient crust at high temperature and low pressure, inferred to have occurred within an extensional tectonic setting.

(4) Magmatic events of this age are unique within the Yangtze Block, suggesting an independent Paleoproterozoic crustal history of the Phan Si Pan Complex relative to other crustal provinces of the Yangtze Block.

(5) The similar tectonothermal history of north Vietnam and the Arrowsmith Orogen of the Rae craton of Laurentia, suggest a close spatial relationship between the two continental blocks in the early Paleoproterozoic.

Acknowledgements

This study was financially supported by projects from the China Natural Science Foundation (41672222) and State Key Laboratory of Geological Process and Mineral Resources, China University of Geosciences, Wuhan (MSFGPMR201802). PAC acknowledges support from Australian Research Council grant FL160100168. This study was also supported by the

Ministry of Natural Resources and Environment of Viet Nam, Project BĐKH.29/16-20 to Dung My Tran. We thank Prof. Guochun Zhao for her editorial handling and three reviewers for their constructive comments that have greatly improved the manuscript.

References

Anderson, I.C., Frost, C.D., Frost, B.R., 2003. Petrogenesis of the Red Mountain pluton, Laramie anorthosite complex, Wyoming: implications for the origin of A-type granite. Precambrian Research 124, 243–267.

Anh, H.T.H., Hieu, P.T., Tu, V.L., Son, L.M., Choi, S.H., Yu, Y., 2015. Age and tectonic implications of Paleoproterozoic Deo Khe Granitoids within the Phan Si Pan Zone, Vietnam. Journal of Asian Earth Sciences 111, 781–791.

Atherton, M.P., Petford, N., 1993. Generation of sodium-rich magmas from newly underplated basaltic crust. Nature 362, 144.

Barbarin, B., 1996. Genesis of the two main types of peraluminous granitoids. Geology 24, 295–298.

Bédard, J., 1990. Enclaves from the A-type granite of the Mégantic Complex, White Mountain Magma Series: Clues to granite magmagenesis. Journal of Geophysical Research: Solid Earth 95, 17797–17819.

Berman, R.G., Pehrsson, S., Davis, W.J., Ryan, J.J., Qui, H., Ashton, K.E., 2013. The Arrowsmith orogeny: Geochronological and thermobarometric constraints on its extent and tectonic setting in the Rae craton, with implications for pre-Nuna supercontinent reconstruction. Precambrian Research 232, 44–69.

Blichert-Toft, J., Chauvel, C., Albarède, F., 1997. Separation of Hf and Lu for high-precision isotope analysis of rock samples by magnetic sector-multiple collector ICP-MS. Contributions to Mineralogy and Petrology 127, 248–260.

Bonin, B., 2007. A-type granites and related rocks: Evolution of a concept, problems and prospects. Lithos 97, 1–29.

Cawood, P. A., Zhao, G., Yao, J., Wang, W., Xu, Y., & Wang, Y., 2018. Reconstructing South China in phanerozoic and precambrian supercontinents. Earth-Science Reviews, 186, 173-194.

Chappell, B.W., 1999. Aluminium saturation in I- and S-type granites and the characterization of fractionated haplogranites. Lithos 46, 535–551.

Chappell, B.W., Bryant, C.J., Wyborn, D., 2012. Peraluminous I-type granites. Lithos 153, 142–153.

Chappell, B.W., Bryant, C.J., Wyborn, D., White, A.J.R., Williams, I.S., 1998. High- and Low-Temperature I-type Granites. Resource Geology 48, 225–235.

Chappell, B.W., White, A.J.R., 1992. I- and S-type granites in the Lachlan Fold Belt. Transactions of the Royal Society of Edinburgh: Earth Sciences 83, 1–26.

Chappell, B.W., White, A.J.R., Williams, I.S., Wyborn, D., 2004. Low- and high-temperature granites. Earth and Environmental Science Transactions of The Royal Society of Edinburgh 95, 125–140.

Chen, W.T., Zhou, M.F., Zhao, X.F., 2013. Late Paleoproterozoic sedimentary and mafic rocks in the Hekou area, SW China: Implication for the reconstruction of the Yangtze Block in Columbia. Precambrian Research 231, 61–77.

Chen, Y., Pei, X., Li, Z., Li, R., Liu, C., Wang, M., 2017. Magmatic events recorded in granitic gneisses from the Hatu area, eastern East Kunlun Orogen: Response to the assembly of Rodinia. Geological Journal 52, 403–418.

Chen, Z.H., Xing, G.F., 2016. Geochemical and zircon U–Pb–Hf–O isotopic evidence for a coherent Paleoproterozoic basement beneath the Yangtze Block, South China. Precambrian Research 279, 81–90.

Clemens, J.D., 2003. S-type granitic magmas—petrogenetic issues, models and evidence. Earth-Science Reviews 61, 1–18.

Collins, W.J., Beams, S.D., White, A.J.R., Chappell, B.W., 1982. Nature and origin of A-type granites with particular reference to southeastern Australia. Contr. Mineral. and Petrol. 80, 189–200.

Condie, K.C., Belousova, E., Griffin, W.L., Sircombe, K.N., 2009. Granitoid events in space and time: Constraints from igneous and detrital zircon age spectra. Gondwana Research 15, 228–242.

Creaser, R.A., Price, R.C., Wormald, R.J., 1991. A-type granites revisited: Assessment of a residual-source model. Geology 19, 163.

Diwu, C., Sun, Y., Zhao, Y., Lai, S., 2014. Early Paleoproterozoic (2.45–2.20Ga) magmatic activity during the period of global magmatic shutdown: Implications for the crustal evolution of the southern North China Craton. Precambrian Research 255, 627–640.

Dong, S.W., Zhang, Y.Q., Gao, R., Su, J.B., Liu, M., Li, J.H., 2015. A possible buried Paleoproterozoic collisional orogen beneath central South China: Evidence from seismic-reflection profiling. Precambrian Research 264, 1–10.

Drummond, M. S., & Defant, M. J., 1990. A model for trondhjemite ‐ tonalite ‐ dacite genesis and crustal growth via slab melting: Archean to modern comparisons. Journal of Geophysical Research: Solid Earth, 95(B13), 21503-21521.

Dos Santos, T.J.S., Fetter, A.H., Van Schmus, W.R., Hackspacher, P.C., 2009. Evidence for 2.35 to 2.30 Ga juvenile crustal growth in the northwest Borborema Province, NE Brazil. Geological Society, London, Special Publications 323, 271–281.

ACCEPTED MANUSCRIPT

Eby, G.N., 1992. Chemical subdivision of the A-type granitoids:Petrogenetic and tectonic implications. Geology 20, 641.

Evans, D. A. D., Li, Z. X., & Murphy, J. B., 2016. Four-dimensional context of Earth's supercontinents. Geological Society, London, Special Publications, 424, SP424-12.

Ferreira, V.P., Sial, A.N., Pimentel, M.M., Armstrong, R., Guimarães, I.P., da Silva Filho, A.F., de Lima, M.M.C., da Silva, T.R., 2015. Reworked old crust-derived shoshonitic magma: The Guarany pluton, Northeastern Brazil. Lithos 232, 150–161.

French, J.E., Heaman, L.M., 2010. Precise U–Pb dating of Paleoproterozoic mafic dyke swarms of the Dharwar craton, India: Implications for the existence of the Neoarchean supercraton Sclavia. Precambrian Research 183, 416–441.

Frost, B.R., Barnes, C.G., Collins, W.J., Arculus, R.J., Ellis, D.J., Frost, C.D., 2001. A Geochemical Classification for Granitic Rocks. Journal of Petrology 42, 2033–2048.

Frost, C.D., Frost, B.R., 2011. On Ferroan (A-type) Granitoids: their Compositional Variability and Modes of Origin. Journal of Petrology 52, 39–53.

Giese, U., Glasmacher, U., Kozlov, V.I., Matenaar, I., Puchkov, V.N., Stroink, L., Bauer, W., Ladage, S., Walter, R., 1999. Structural framework of the Bashkirian anticlinorium, SW Urals. Geologische Rundschau 87, 526–544.

Gong, S., Chen, N., Geng, H., Sun, M., Zhang, L., Wang, Q., 2014. Zircon Hf isotopes and geochemistry of the early paleoproterozoic high-Sr low-y quartz-diorite in the Quanji massif, NW China: Crustal growth and tectonic implications. Journal of Earth Science 25, 74–86.

Greentree, M.R., Li, Z. X., 2008. The oldest known rocks in south–western China: SHRIMP U–Pb magmatic crystallisation age and detrital provenance analysis of the Paleoproterozoic Dahongshan Group. Journal of Asian Earth Sciences 33, 289–302.

Griffin, W.L., Belousova, E.A., Walters, S.G., O'Reilly, S.Y., 2006. Archaean and Proterozoic crustal evolution in the Eastern Succession of the Mt Isa district, Australia: U–Pb and Hf-isotope studies of detrital zircons. Australian Journal of Earth Sciences 53, 125–149.

Gromet, P., Silver, L.T., 1987. REE Variations Across the Peninsular Ranges Batholith: Implications for Batholithic Petrogenesis and Crustal Growth in Magmatic Arcs. Journal of Petrology 28, 75–125.

Guo, J. L., Gao, S., Wu, Y. B., Li, M., Chen, K., Hu, Z. C., Liang, Z. W., Liu, Y. S., Zhou, L., Zong, K. Q., Zhang, W., Chen, H. H., 2014. 3.45Ga granitic gneisses from the Yangtze Craton, South China: Implications for Early Archean crustal growth. Precambrian Research 242, 82–95.

Han, Q., Peng, S., Kusky, T., Polat, A., Jiang, X., Cen, Y., Liu, S., Deng, H., 2017. A Paleoproterozoic ophiolitic mélange, Yangtze craton, South China: Evidence for Paleoproterozoic suturing and microcontinent amalgamation. Precambrian Research 293, 13–38.

Han, Q., Peng, S., Polat, A., Kusky, T., Deng, H., Wu, T., 2018. A ca.2.1 Ga Andean-type margin built on metasomatized lithosphere in the northern Yangtze craton, China: Evidence from high-Mg basalts and andesites. Precambrian Research 309, 309–324.

Hartlaub, R.P., Heaman, L.M., Chacko, T., Ashton, K.E., 2007. Circa 2.3-Ga Magmatism of the Arrowsmith Orogeny, Uranium City Region, Western Churchill Craton, Canada. The Journal of Geology 115, 181–195.

He, C., Gong, S., Wang, L., Chen, N., Santosh, M., Wang, Q., 2018. Protracted post-collisional magmatism during plate subduction shutdown in early Paleoproterozoic: Insights from post-collisional granitoid suite in NW China. Gondwana Research 55, 92–111.

Hieu, P.T., Chen, F., Me, L.T., Thuy, N.T.B., Siebel, W., Lan, T. G., 2012. Zircon U–Pb ages and Hf isotopic compositions from the Sin Quyen Formation: the Precambrian crustal evolution of northwest Vietnam. International Geology Review 54, 1548–1561.

Hieu, P.T., Dung, N.T., Nguyen, T.B.T., Minh, N.T., Minh, P., 2016. U–Pb ages and Hf isotopic composition of zircon and bulk rock geochemistry of the Dai Loc granitoid complex in Kontum massif: Implications for early Paleozoic crustal evolution in Central Vietnam. Journal of Mineralogical and Petrological Sciences 111, 326–336.

Hsu, S. K., Sibuet, J.C., 1995. Is Taiwan the result of arc-continent or arc-arc collision? Earth and Planetary Science Letters 136, 315–324.

Hu, Z., Liu, Y., Gao, S., Xiao, S., Zhao, L., Günther, D., Li, M., Zhang, W., Zong, K., 2012. A “wire” signal smoothing device for laser ablation inductively coupled plasma mass spectrometry analysis. Spectrochimica Acta Part B: Atomic Spectroscopy 78, 50–57.

Hu, J., Liu, X., Chen, L., Qu, W., Li, H., Geng, J., 2013. A ~2.5 Ga magmatic event at the northern margin of the Yangtze craton: Evidence from U-Pb dating and Hf isotope analysis of zircons from the Douling Complex in the South Qinling orogen. Chinese Science Bulletin 58, 3564–3579.

Hui, B., Dong, Y., Cheng, C., Long, X., Liu, X., Yang, Z., Sun, S., Zhang, F., Varga, J., 2017. Zircon U–Pb chronology, Hf isotope analysis and whole-rock geochemistry for the Neoarchean-Paleoproterozoic Yudongzi complex, northwestern margin of the Yangtze craton, China. Precambrian Research 301, 65–85.

Huang, H.Q., Li, X.H., Li, W.X., Li, Z.X., 2011. Formation of high ^{18}O fayalite-bearing A-type granite by high-temperature melting of granulitic metasedimentary rocks, southern China. Geology 39, 903–906.

Huang, X.L., Wilde, S.A., Zhong, J. W., 2013. Episodic crustal growth in the southern segment of the Trans-North China Orogen across the Archean-Proterozoic boundary. Precambrian Research 233, 337–357.

Jiao, W., Wu, Y., Yang, S., Peng, M., Wang, J., 2009. The oldest basement rock in the Yangtze Craton revealed by zircon U-Pb age and Hf isotope composition. Science in China Series D: Earth Sciences 52, 1393–1399.

King, P.L., White, A.J.R., Chappell, B.W., Allen, C.M., 1997. Characterization and Origin of Aluminous A-type Granites from the Lachlan Fold Belt, Southeastern Australia 38, 21.

Kou, C., Zhang, Z., Santosh, M., Huang, H., Zhu, J., 2017. Oldest volcanic-hosted submarine iron ores in South China: Evidence from zircon U–Pb geochronology and geochemistry of the Paleoproterozoic Dahongshan iron deposit. Gondwana Research 49, 182–204.

Kröner, A., Wilde, S.A., Li, J.H., Wang, K.Y., 2005. Age and evolution of a late Archean to Paleoproterozoic upper to lower crustal section in the Wutaishan/Hengshan/Fuping terrain of northern China. Journal of Asian Earth Sciences 24, 577–595.

Kullerud, K., Skjerlie, K.P., Corfu, F., de la Rosa, J.D., 2006. The 2.40Ga Ringvassøy mafic dykes, West Troms Basement Complex, Norway: The concluding act of early Palaeoproterozoic continental breakup. Precambrian Research 150, 183–200.

Kumar, A., Hamilton, M.A., Halls, H.C., 2012. A Paleoproterozoic giant radiating dyke swarm in the Dharwar Craton, southern India: Dharwar Giant Dyke Swarm. Geochemistry, Geophysics, Geosystems 13

Lan, C.Y., Chung, S.L., Lo, C.H., Lee, T.Y., Wang, P.L., Li, H., Van Toan, D., 2001. First evidence for Archean continental crust in northern Vietnam and its implications for crustal and tectonic evolution in Southeast Asia. Geology 29, 219–222.

ACCEPTED MANUSCRIPT

Laurent, O., Martin, H., Moyen, J.F., Doucelance, R., 2014. The diversity and evolution of late-Archean granitoids: Evidence for the onset of “modern-style” plate tectonics between 3.0 and 2.5Ga. Lithos 205, 208–235.

Li, X. C., Zhao, J. H., Zhou, M. F., Gao, J. F., Sun, W. H., Tran, M., 2018. Neoproterozoic granitoids from the Phan Si Pan belt, Northwest Vietnam: Implication for the tectonic linkage between Northwest Vietnam and the Yangtze Block. Precambrian Research 309, 212–230.

Li, L., Lin, S., Davis, D.W., Xiao, W., Xing, G., Yin, C., 2014. Geochronology and geochemistry of igneous rocks from the Kongling terrane: Implications for Mesoarchean to Paleoproterozoic crustal evolution of the Yangtze Block. Precambrian Research 255, 30–47.

Li, Y., Zheng, J., Xiong, Q., Wang, W., Ping, X., Li, X., Tang, H., 2016. Petrogenesis and tectonic implications of Paleoproterozoic metapelitic rocks in the Archean Kongling Complex from the northern Yangtze Craton, South China. Precambrian Research 276, 158–177.

Liu, Y., Hu, Z., Gao, S., Günther, D., Xu, J., Gao, C., Chen, H., 2008. In situ analysis of major and trace elements of anhydrous minerals by LA-ICP-MS without applying an internal standard. Chemical Geology 257, 34–43.

Liu, Y., Hu, Z., Zong, K., Gao, C., Gao, S., Xu, J., Chen, H., 2010. Reappraisement and refinement of zircon U-Pb isotope and trace element analyses by LA-ICP-MS. Chinese Science Bulletin 55, 1535–1546.

Ludwig, K.R., 2003. User’s manual for IsoPlot 3.0. A Geochronological Toolkit for Microsoft Excel 71.

Luo, B., Liu, R., Zhang, H., Zhao, J., Yang, H., Xu, W., Guo, L., Zhang, L., Tao, L., Pan, F., Wang, W., Gao, Z., Shao, H., 2018. Neoproterozoic continental back-arc rift development in the Northwestern Yangtze Block: Evidence from the Hannan intrusive magmatism. Gondwana Research.

Macambira, M.J.B., Vasquez, M.L., Silva, D.C.C. da, Galarza, M.A., Barros, C.E. de M., Camelo, J. de F., 2009. Crustal growth of the central-eastern Paleoproterozoic domain, SW Amazonian craton: Juvenile accretion vs. reworking. Journal of South American Earth Sciences 27, 235–246.

Manyeruke, T.D., Blenkinsop, T.G., Buchholz, P., Love, D., Oberthür, T., Vetter, U.K., Davis, D.W., 2004. The age and petrology of the Chimbadzi Hill Intrusion, NW Zimbabwe: first evidence for early Paleoproterozoic magmatism in Zimbabwe. Journal of African Earth Sciences 40, 281–292.

Martin, H., Smithies, R.H., Rapp, R., Moyen, J.F., Champion, D., 2005. An overview of adakite, tonalite–trondhjemite–granodiorite (TTG), and sanukitoid: relationships and some implications for crustal evolution. Lithos 79, 1–24.

McCulloch, M.T., Rosman, K.J., De Laeter, J.R., 1977. The isotopic and elemental abundance of ytterbium in meteorites and terrestrial samples. Geochimica et Cosmochimica Acta 41, 1703–1707.

Miller, C.F., McDowell, S.M., Mapes, R.W., 2003. Hot and cold granites? Implications of zircon saturation temperatures and preservation of inheritance. Geology 31, 529.

Mukherjee, S., Dey, A., Ibanez-Mejia, M., Sanyal, S., Sengupta, P., 2018. Geochemistry, U-Pb geochronology and Lu-Hf isotope systematics of a suite of ferroan (A-type) granitoids from the CGGC: Evidence for Mesoproterozoic crustal extension in the east Indian shield. Precambrian Research 305, 40–63.

Mushkin, A., Navon, O., Halicz, L., Hartmann, G., Stein, M., 2003. The petrogenesis of A-type magmas from the Amram Massif, southern Israel. Journal of Petrology 44, 815–832.

Middlemost, E.A., 1994. Naming materials in the magma/igneous rock system. Earth-Science Reviews 37, 215–224.

Nagel, T.J., Hoffmann, J.E., Münker, C., 2012. Generation of Eoarchean tonalite-trondhjemite-granodiorite series from thickened mafic arc crust. Geology 40, 375–378.

Nam, T. N., Toriumi, M., & Itaya, T. 1998. P–T–t paths and post-metamorphic exhumation of the Day Nui Con Voi shear zone in Vietnam. Tectonophysics, 290(3-4), 299-318.

Nam, T.N., Toriumi, M., Sano, Y., Terada, K., Thang, T.T., 2003. 2.9, 2.36, and 1.96 Ga zircons in orthogneiss south of the Red River shear zone in Viet Nam: evidence from SHRIMP U–Pb dating and tectonothermal implications. Journal of Asian Earth Sciences 21, 743–753.

Nilsson, M.K.M., Klausen, M.B., Söderlund, U., Ernst, R.E., 2013. Precise U–Pb ages and geochemistry of Palaeoproterozoic mafic dykes from southern West Greenland: Linking the North Atlantic and the Dharwar cratons. Lithos 174, 255–270.

Nie, H., Yao, J., Wan, X., Zhu, X.Y., Siebel, W., Chen, F., 2016. Precambrian tectonothermal evolution of South Qinling and its affinity to the Yangtze Block: Evidence from zircon ages and Hf-Nd isotopic compositions of basement rocks. Precambrian Research 286, 167–179.

O'Neill, C., Lenardic, A., Moresi, L., Torsvik, T.H., Lee, C.-T.A., 2007. Episodic Precambrian subduction. Earth and Planetary Science Letters 262, 552–562.

Partin, C.A., Bekker, A., Sylvester, P.J., Wodicka, N., Stern, R.A., Chacko, T., Heaman, L.M., 2014. Filling in the juvenile magmatic gap: Evidence for uninterrupted Paleoproterozoic plate tectonics. Earth and Planetary Science Letters 388, 123–133.

Patiño Douce, A.E., 1997. Generation of metaluminous A-type granites by low-pressure melting of calc-alkaline granitoids. Geology 25, 743.

Patiño Douce, A.E., Beard, J.S., 1995. Dehydration-melting of Biotite Gneiss and Quartz Amphibolite from 3 to 15 kbar. Journal of Petrology 36, 707–738.

Pehrsson, S.J., Buchan, K.L., Eglington, B.M., Berman, M., Rainbird, R.H., 2014. Did plate tectonics shutdown in the Paleoproterozoic? A view from the Siderian geologic record. Gondwana Research. 26, 803–815.

Pearce, J.A., Harris, N.B., Tindle, A.G., 1984. Trace element discrimination diagrams for the tectonic interpretation of granitic rocks. Journal of petrology 25, 956–983.

Polat, A., Hofmann, A., 2003. Alteration and geochemical patterns in the 3.7–3.8 Ga Isua greenstone belt, West Greenland. Precambrian Research 126, 197–218.

Rapp, R.P., Watson, E.B., 1995. Dehydration melting of metabasalt at 8–32 kbar: implications for continental growth and crust-mantle recycling. Journal of Petrology 36, 891–931.

Rogers, J.J., Greenberg, J.K., 1990. Late-orogenic, post-orogenic, and anorogenic granites: distinction by major-element and trace-element chemistry and possible origins. The Journal of Geology 98, 291–309.

Rogers, J.J., Santosh, M., 2002. Configuration of Columbia, a Mesoproterozoic supercontinent. Gondwana Research 5, 5–22.

Rollinson, H., Martin, H., 2005. Geodynamic controls on adakite, TTG and sanukitoid genesis: implications for models of crust formation. Lithos 79, ix–xii.

Rossignol, C., Bourquin, S., Hallot, E., Poujol, M., Dabard, M.-P., Martini, R., Villeneuve, M., Cornée, J.-J., Brayard, A., Roger, F., 2018. The indosinian orogeny: A perspective from sedimentary archives of north Vietnam. Journal of Asian Earth Sciences.

Rickwood, P.C., 1989. Boundary lines within petrologic diagrams which use oxides of major and minor elements. Lithos 22, 247–263.

Santosh, M., Yang, Q.Y., Teng, X., Tang, L., 2015. Paleoproterozoic crustal growth in the North China Craton: Evidence from the Lüliang Complex. Precambrian Research 263, 197–231.

Scherer, E., Münker, C., Mezger, K., 2001. Calibration of the lutetium-hafnium clock. Science 293, 683–687.

Seixas, L.A.R., David, J., Stevenson, R., 2012. Geochemistry, Nd isotopes and U–Pb geochronology of a 2350Ma TTG suite, Minas Gerais, Brazil: Implications for the crustal evolution of the southern São Francisco craton. Precambrian Research 196–197, 61–80.

Sisson, T.W., Ratajeski, K., Hankins, W.B., Glazner, A.F., 2005. Voluminous granitic magmas from common basaltic sources. Contributions to Mineralogy and Petrology 148, 635–661.

Spencer, C.J., Murphy, J.B., Kirkland, C.L., Liu, Y., Mitchell, R.N., 2018. A Palaeoproterozoic tectono-magmatic lull as a potential trigger for the supercontinent cycle. Nature Geoscience 11, 97–101.

Stepanova, A.V., Salnikova, E.B., Samsonov, A.V., Egorova, S.V., Larionova, Y.O., Stepanov, V.S., 2015. The 2.31Ga mafic dykes in the Karelian Craton, eastern Fennoscandian shield: U–Pb age, source characteristics and implications for continental break-up processes. Precambrian Research 259, 43–57.

Sun, S. S., McDonough, W.F., 1989. Chemical and isotopic systematics of oceanic basalts: implications for mantle composition and processes. Geological Society, London, Special Publications 42, 313–345.

Tchameni, R., Mezger, K., Nsifa, N. E., Pouclet, A., 2001. Crustal origin of Early Proterozoic syenites in the Congo craton (Ntem complex), South Cameroon. Lithos, 57(1), 23-42.

Teixeira, W., Ávila, C.A., Dussin, I.A., Corrêa Neto, A.V., Bongiolo, E.M., Santos, J.O., Barbosa, N.S., 2015. A juvenile accretion episode (2.35–2.32Ga) in the Mineiro belt and its role to the Minas accretionary orogeny: Zircon U–Pb–Hf and geochemical evidences. Precambrian Research 256, 148–169.

Turner, S.P., Foden, J.D., Morrison, R.S., 1992. Derivation of some A-type magmas by fractionation of basaltic magma: an example from the Padthaway Ridge, South Australia. Lithos 28, 151–179.

Usuki, T., Lan, C.Y., Tran, T.H., Pham, T.D., Wang, K.L., Shellnutt, G.J., Chung, S.L., 2015. Zircon U–Pb ages and Hf isotopic compositions of alkaline silicic magmatic rocks in the Phan Si Pan-Tu Le region, northern Vietnam: Identification of a displaced western extension of the Emeishan Large Igneous Province. Journal of Asian Earth Sciences 97, 102–124.

Watson, E.B., Harrison, T.M., 1983. Zircon saturation revisited: temperature and composition effects in a variety of crustal magma types. Earth and Planetary Science Letters 64, 295–304.

Wang, Z., Wang, J., Du, Q., Deng, Q., Yang, F., Wu, H., 2013. Mature Archean continental crust in the Yangtze craton: evidence from petrology, geochronology and geochemistry. Chinese Science Bulletin 58, 2360–2369.

Wang, K., Dong, S., Li, Z. X., Han, B., 2018a. Age and chemical composition of Archean metapelites in the Zhongxiang Complex and implications for early crustal evolution of the Yangtze Craton. Lithos 320–321, 280–301. https://doi.org/10.1016/j.lithos.2018.09.027

Wang, K., Li, Z. X., Dong, S., Cui, J., Han, B., Zheng, T., Xu, Y., 2018b. Early crustal evolution of the Yangtze Craton, South China: New constraints from zircon U-Pb-Hf isotopes and geochemistry of ca. 2.9–2.6 Ga granitic rocks in the Zhongxiang Complex. Precambrian Research. 314, 325-352.

Wang, Z., Deng, Q., Duan, T., Yang, F., Du, Q., Xiong, X., Liu, H., Cao, B., 2018c. 2.85 Ga and 2.73 Ga A-type granites and 2.75 Ga trondhjemite from the Zhongxiang Terrain: Implications for early crustal evolution of the Yangtze Craton, South China. Gondwana Research 61, 1–19.

Wang, W., Cawood, P.A., Zhou, M. F., Zhao, J. H., 2016. Paleoproterozoic magmatic and metamorphic events link Yangtze to northwest Laurentia in the Nuna supercontinent. Earth and Planetary Science Letters 433, 269–279.

Wang, Z., Wang, J., Deng, Q., Du, Q., Zhou, X., Yang, F., Liu, H., 2015. Paleoproterozoic I-type granites and their implications for the Yangtze block position in the Columbia supercontinent: Evidence from the Lengshui Complex, South China. Precambrian Research 263, 157–173.

Whalen, J.B., Currie, K.L., Chappell, B.W., 1987. A-type granites: geochemical characteristics, discrimination and petrogenesis. Contributions to Mineralogy and Petrology 95, 407–419.

Wu, F., Sun, D., Li, H., Jahn, B., Wilde, S., 2002. A-type granites in northeastern China: age and geochemical constraints on their petrogenesis. Chemical Geology 187, 143–173.

Wu, F.Y., 2007. Discussions on the petrogenesis of granites. Acta Petrologica Sinica 23, 1217–1238.

Wu, G., Xiao, Y., Bonin, B., Ma, D., Li, X., Zhu, G., 2018. Ca. 850 Ma magmatic events in the Tarim Craton: Age, geochemistry and implications for assembly of Rodinia supercontinent. Precambrian Research 305, 489–503.

Wu, Y., Gao, S., Zhang, H., Zheng, J., Liu, X., Wang, H., Gong, H., Zhou, L., Yuan, H., 2012. Geochemistry and zircon U–Pb geochronology of Paleoproterozoic arc related granitoid in the Northwestern Yangtze Block and its geological implications. Precambrian Research 200–203, 26–37.

Wu, Y.B., Zheng, Y.F., Gao, S., Jiao, W.F., Liu, Y.S., 2008. Zircon U–Pb age and trace element evidence for Paleoproterozoic granulite-facies metamorphism and Archean crustal rocks in the Dabie Orogen. Lithos 101, 308–322.

Winchester, J. A., Floyd, P. A., 1976. Geochemical magma type discrimination: application to altered and metamorphosed basic ignecous rocks. Earth and Planetary Science Letters, 28(3), 459-469.

Xiong, Q., Zheng, J., Yu, C., Su, Y., Tang, H., Zhang, Z., 2009. Zircon U-Pb age and Hf isotope of Quanyishang A-type granite in Yichang: signification for the Yangtze continental cratonization in Paleoproterozoic. Science Bulletin 54, 436–446.

Xiong, X., Gao, R., Wang, H., Zhang, J., Guo, L., 2016. Frozen subduction in the Yangtze block: insights from the deep seismic profiling and gravity anomaly in east Sichuan fold belt. Earthquake Science 29, 61–70.

Yang, J.H., Wu, F.Y., Chung, S.L., Wilde, S.A., Chu, M. F., 2006. A hybrid origin for the Qianshan A-type granite, northeast China: Geochemical and Sr–Nd–Hf isotopic evidence. Lithos 89, 89–106.

Yang, Z.N., Yang, K.G., Polat, A., Xu, Y., 2018. Early crustal evolution of the eastern Yangtze Block: Evidence from detrital zircon U-Pb ages and Hf isotopic composition of the Neoproterozoic Huashan Group in the Dahongshan area. Precambrian Research 309, 248–270.

Yin, C., Lin, S., Davis, D.W., Zhao, G., Xiao, W., Li, L., He, Y., 2013. 2.1–1.85Ga tectonic events in the Yangtze Block, South China: Petrological and geochronological evidence from the Kongling Complex and implications for the reconstruction of supercontinent Columbia. Lithos 182–183, 200–210.

Yuan, L., Zhang, X., Yang, Z., Lu, Y., Chen, H., 2017. Paleoproterozoic Alaskan-type ultramafic–mafic intrusions in the Zhongtiao mountain region, North China Craton: Petrogenesis and tectonic implications. Precambrian Research 296, 39–61.

Zhang, C.L., Li, Z.X., Li, X.H., Yu, H.F., Ye, H-M., 2007. An early Paleoproterozoic high-K intrusive complex in southwestern Tarim Block, NW China: Age, geochemistry, and tectonic implications. Gondwana Research 12, 101–112.

Zhang, R., Murphy, M. A., Lapen, T. J., Sanchez, V., Heizler, M., 2011. Late Eocene crustal thickening followed by Early-Late Oligocene extension along the India-Asia suture zone: Evidence for cyclicity in the Himalayan orogen. Geosphere, 7(5), 1249-1268.

Zhang, S.B., Zheng, Y.F., Wu, Y.-B., Zhao, Z.F., Gao, S., Wu, F.Y., 2006. Zircon U–Pb age and Hf isotope evidence for 3.8 Ga crustal remnant and episodic reworking of Archean crust in South China. Earth and Planetary Science Letters 252, 56–71.

Zhang, R.Y., Lo, C.H., Chung, S.L., Grove, M., Omori, S., Iizuka, Y., Liou, J.G., Tri, T.V., 2013. Origin and Tectonic Implication of Ophiolite and Eclogite in the Song Ma Suture Zone between the South China and Indochina Blocks: origin of the song ma ophiolite and eclogite. Journal of Metamorphic Geology 31, 49–62.

Zhao, G., Cawood, P.A., Wilde, S.A., Sun, M., 2002. Review of global 2.1–1.8 Ga orogens: implications for a pre-Rodinia supercontinent. Earth-Science Reviews 59, 125–162.

Zhao, G., Sun, M., Wilde, S.A., Li, S., 2003. Assembly, Accretion and Breakup of the Paleo-Mesoproterozoic Columbia Supercontinent: Records in the North China Craton 6, 417–434.

Zhao, G., Wilde, S.A., Sun, M., Li, S., Li, X., Zhang, J., 2008a. SHRIMP U–Pb zircon ages of granitoid rocks in the Lüliang Complex: Implications for the accretion and evolution of the Trans-North China Orogen. Precambrian Research 160, 213–226.

Zhao, J. H., Zhang, S. B., Wang, X. L., 2018a. Neoproterozoic geology and reconstruction of South China. Precambrian Research. 309, 1-5.

Zhao, X.F., Zhou, M.F., Li, J.W., Sun, M., Gao, J.F., Sun, W.H., Yang, J.H., 2010. Late Paleoproterozoic to early Mesoproterozoic Dongchuan Group in Yunnan, SW China: Implications for tectonic evolution of the Yangtze Block. Precambrian Research 182, 57–69.

Zhao, X.F., Zhou, M.F., Li, J.W., Wu, F.Y., 2008b. Association of Neoproterozoic A- and I-type granites in South China: Implications for generation of A-type granites in a subduction-related environment. Chemical Geology 257, 1–15.

Zhao, Y., Li, N., Jiang, Y., Niu, H., 2017. Petrogenesis of the Late Archean (~2.5 Ga) Na- and K-rich granitoids in the Zhongtiao-Wangwu region and its tectonic significance for the crustal evolution of the North China Craton. Precambrian Research 303, 590–603.

Zhao, Z.F., Gao, P., Zheng, Y.F., 2015. The source of Mesozoic granitoids in South China: Integrated geochemical constraints from the Taoshan batholith in the Nanling Range. Chemical Geology 395, 11–26.

Zhou, G., Wu, Y., Wang, H., Qin, Z., Zhang, W., Zheng, J., Yang, S., 2017. Petrogenesis of the Huashanguan A-type granite complex and its implications for the early evolution of the Yangtze Block. Precambrian Research 292, 57–74.

Zhou, M.F., Zhao, X.F., Chen, W.T., Li, X.C., Wang, W., Yan, D.P., Qiu, H.N., 2014. Proterozoic Fe–Cu metallogeny and supercontinental cycles of the southwestern Yangtze Block, southern China and northern Vietnam. Earth-Science Reviews 139, 59–82.

Zhou, B. G., Wang, S. W., Sun, X. M., Liao, Z. W., Guo, Y., Jiang, X. F., Shen, Z. W., 2012. SHRIMP U–Pb age and its significance of zircons in welded tuff of Wangchang formation in Dongchuan area, Yunnan Province, SW China. Geological Review, 58(2), 359-368. (in chinese)

Zhou, G., Wu, Y., Gao, S., Yang, J., Zheng, J., Qin, Z., Wang, H., Yang, S., 2015. The 2.65 Ga A-type granite in the northeastern Yangtze craton: Petrogenesis and geological implications. Precambrian Research 258, 247–259.

Zhu, H. P., Fan, W. Y., Zhou, B. G., Wang, S. W., Luo, M. J., Liao, Z. W., Guo, Y. 2011. Assessing Precambrian stratigraphic sequence of Dongchuan area: evidence from zircon SHRIMP and LA-ICP-MS dating. Geological Journal of China Universities, 17(3), 452-461. (in chinese)

Fig. 1. Simplified regional map highlighting the distribution of Precambrian geological units in the South China Craton (modified after Wang et al. 2018b). Geochronological data sources: Yudongzi Complex (Wu et al., 2012; Hui et al., 2017); Kongling Complex (Jiao et al., 2009; Guo et al., 2014, 2015; Li et al., 2014, 2016; Han et al., 2018); Douling Complex (Hu et al., 2013; Nie et al., 2016); Zhongxiang Complex (Wang et al., 2013; Zhou et al., 2015; Wang et al., 2018a,b,c); Tandang Group (Zhu et al., 2011); Phan Si Pan Complex (Lan et al., 2001; Wang et al., 2016 and this study).

Fig. 2. Simplified geological map of north Vietnam region. ASRR = Ailaoshan-Red River (modified after Usuki et al. 2015 and Wang et al. 2016). Geochronological data cited are from 1: Wang et al. (2016); 2: Lan et al. (2001); 3: Anh et al. (2015).

Fig. 3. Field photographs showing the studied rocks in the Phan Si Pan Complex of in north Vietnam (A for 2.3 Ga quartz monzonites and B for 2.1 Ga gneissic granite). Photomicrographs of the textures and mineralogy of the quartz monzonite (C and D) and gneissic granite (E and F) in the Phan Si Pan Complex. Qtz: quartz; Pl: plagioclase; Bi: biotite; Kfs: K-feldspar.

Fig. 4. Cathodoluminescence (CL) images of representative zircon grains from the Phan Si Pan Complex granitoids showing internal structures and analytical locations. Solid (red) and dashed (yellow) circles indicate the locations of U-Pb dating and Hf analyses, respectively.

Fig. 5. LA-ICP-MS zircon U-Pb age concordia plot of zircons from sample 16VN02-09 and 16VN02-06 (A and C), and the weighted mean age interpreted as the best estimates of the age of the granites (B and D).

Fig. 6. Plot of zircon $\varepsilon_{Hf}(t)$ versus $^{207}Pb/^{206}Pb$ age for the Archean-Paleoproterozoic rocks from Yangtze Block. Data are from Zhang et al. (2006); Jiao et al. (2009); Wu et al. (2012); Guo et al. (2014, 2015); Wang et al. (2015, 2018b, 2018c); Zhou et al. (2015); Chen and Xing (2016); Han et al. (2018).

Fig. 7. Geochemical discriminations of the granite samples in (A) Zr/TiO_2 *0.0001 versus Nb/Y plot (Winchester and Floyd, 1976); (B) K_2O versus SiO_2 diagram (Middlemost, 1994); (C) FeOT/(FeO + MgO) versus SiO_2 diagram (Frost et al., 2001). (D) A/NK versus A/CNK diagram (Frost et al. 2001).

Fig. 8. Primitive-mantle normalized trace element spider diagrams and chondrite-normalized REE patterns of the granites from Phan Si Pan Complex. Primitive-mantle and chondrite values from (Sun and McDonough, 1989).

Fig. 9. Plots of the samples in 10000*Ga/Al versus (A) K_2O/MgO, (B) (Na_2O+K_2O)/CaO, (C) Y, and (D) Nb from (Whalen et al., 1987); (E) Ce/Nb versus Y/Nb; (F) Nb–Y–Ce diagram (E and F after Eby, 1992).

Fig. 10. (A) P_2O_5 versus SiO_2 for the quartz monzonite from Phan Si Pan complex.

Fig. 11. (A) Sr/Y vs. Y and (a) $(La/Yb)_N$ vs. $(Yb)_N$ discrimination diagrams for the granites from Phan Si Pan complex. Plots show the typical adakitic characteristics (Drummond and Defant, 1990).

Fig.12. (A) Ta versus Yb discrimination diagram for the granites from Phan Si Pan complex after (Pearce et al., 1984). VAG: volcanic arc granite; ORG: ocean ridge granite; WPG: within-plate granite; syn-COLG: syn-collisional granite.

Fig. 13. Histograms of zircon ages (>1.5 Ga) for rocks from Yangtze Block (Data from (Zhang et al., 2006; Jiao et al., 2009; Peng et al., 2012, 2019; Wu et al., 2012; Chen et al., 2013; Guo et al., 2014, 2015; Anh et al., 2015; Wang et al., 2015, 2018b, c; Hui et al., 2017; Han et al., 2018; Zhou et al., 2017, 2018). n = number of rock samples. The location of the regions are same as Figure 1.

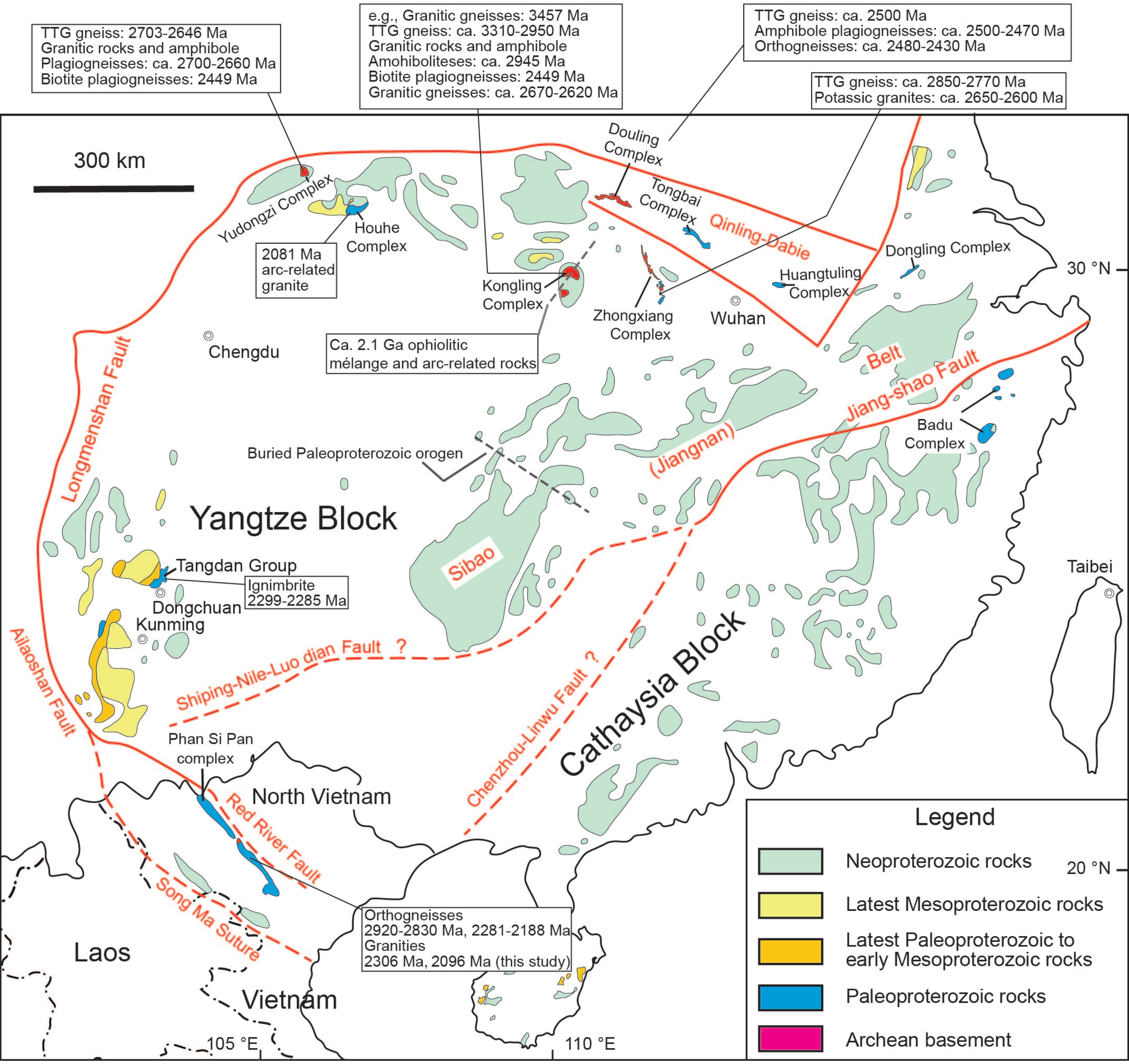

TTG gneiss: 2703-2646 Ma
Granitic rocks and amphibole
Plagiogneisses: ca. 2700-2660 Ma
Biotite plagiogneisses: 2449 Ma
e.g., Granitic gneisses: 3457 Ma
TTG gneiss: ca. 3310-2950 Ma
Granitic rocks and amphibole
Amohiboliteses: ca. 2945 Ma
Biotite plagiogneisses: 2449 Ma
Granitic gneisses: ca. 2670-2620 Ma
TTG gneiss: ca. 2500 Ma
Amphibole plagiogneisses: ca. 2500-2470 Ma
Orthogneisses: ca. 2480-2430 Ma
TTG gneiss: ca. 2850-2770 Ma
Potassic granites: ca. 2650-2600 Ma
300 km
Yudongzi Complex
Houhe Complex
2081 Ma arc-related granite
Douling Complex
Tongbai Complex
Qinling-Dabie
Kongling Complex
Zhongxiang Complex
Wuhan
Dongling Complex
Huangtuling Complex
30 °N
Chengdu
Ca. 2.1 Ga ophiolitic mélange and arc-related rocks
Belt
Jiang-shao Fault
(Jiangnan)
Badu Complex
Longmenshan Fault
Buried Paleoproterozoic orogen
Yangtze Block
Tangdan Group
Ignimbrite 2299-2285 Ma
Dongchuan
Kunming
Sibao
Taibei
Cathaysia Block
Shiping-Nile-Luo dian Fault ?
Chenzhou-Linwu Fault ?
Ailaoshan Fault
Phan Si Pan complex
North Vietnam
Red River Fault
Song Ma Suture
Laos
Vietnam
Orthogneisses
2920-2830 Ma, 2281-2188 Ma
Granities
2306 Ma, 2096 Ma (this study)
105 °E
110 °E
20 °N
Legend
Neoproterozoic rocks
Latest Mesoproterozoic rocks
Latest Paleoproterozoic to early Mesoproterozoic rocks
Paleoproterozoic rocks
Archean basement

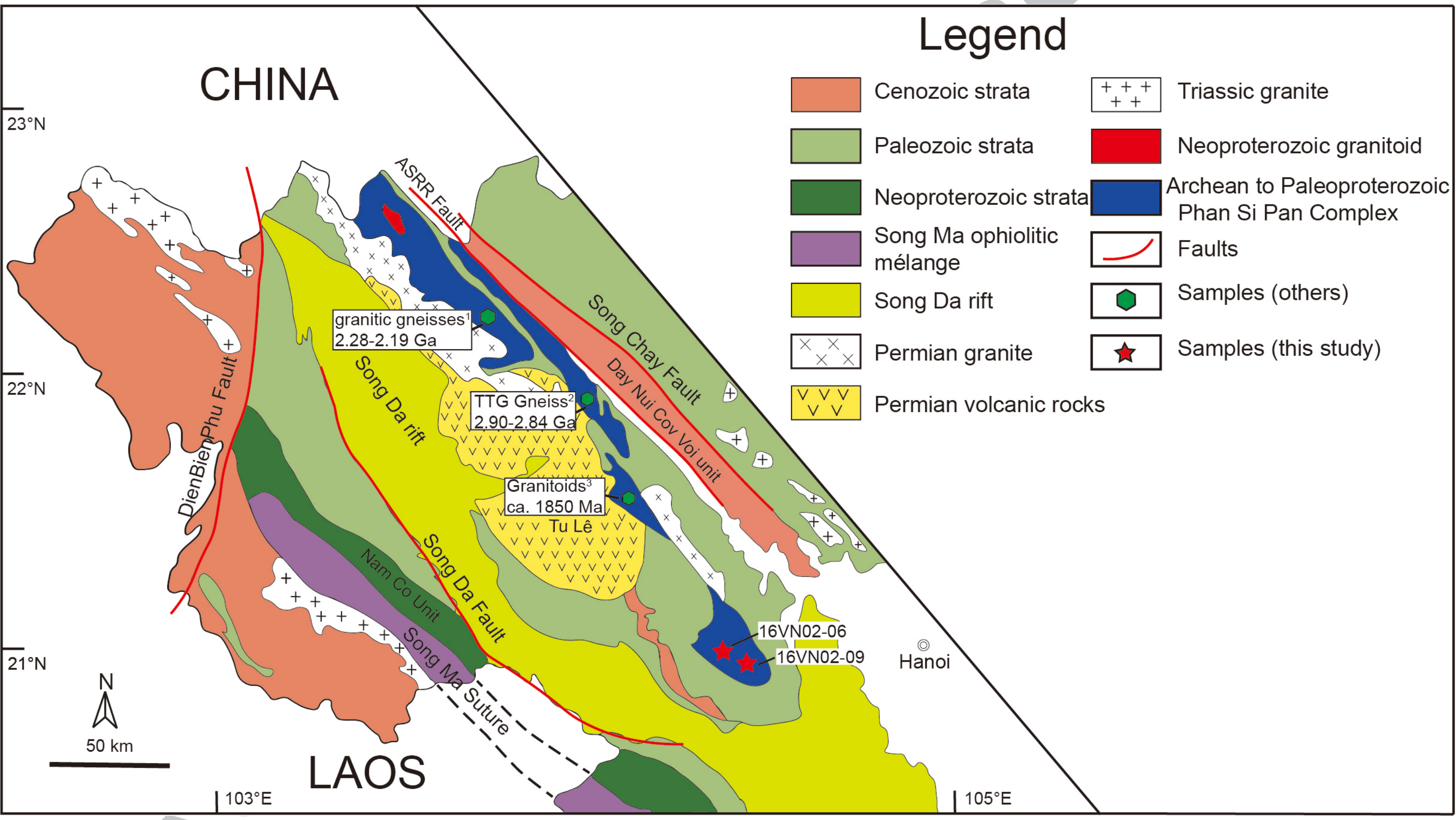

CHINA
LAOS
Legend
Cenozoic strata
Paleozoic strata
Neoproterozoic strata
Song Ma ophiolitic mélange
Song Da rift
Permian granite
Permian volcanic rocks
Triassic granite
Neoproterozoic granitoid
Archean to Paleoproterozoic Phan Si Pan Complex
Faults
Samples (others)
Samples (this study)
23°N
22°N
21°N
103°E
105°E
N
50 km
ASRR Fault
Song Chay Fault
Day Nui Cov Voi unit
DienBienPhu Fault
Song Da rift
Song Da Fault
Nam Co Unit
Song Ma Suture
granitic gneisses[1]
2.28-2.19 Ga
TTG Gneiss[2]
2.90-2.84 Ga
Granitoids[3]
ca. 1850 Ma
Tu Lê
16VN02-06
16VN02-09
Hanoi

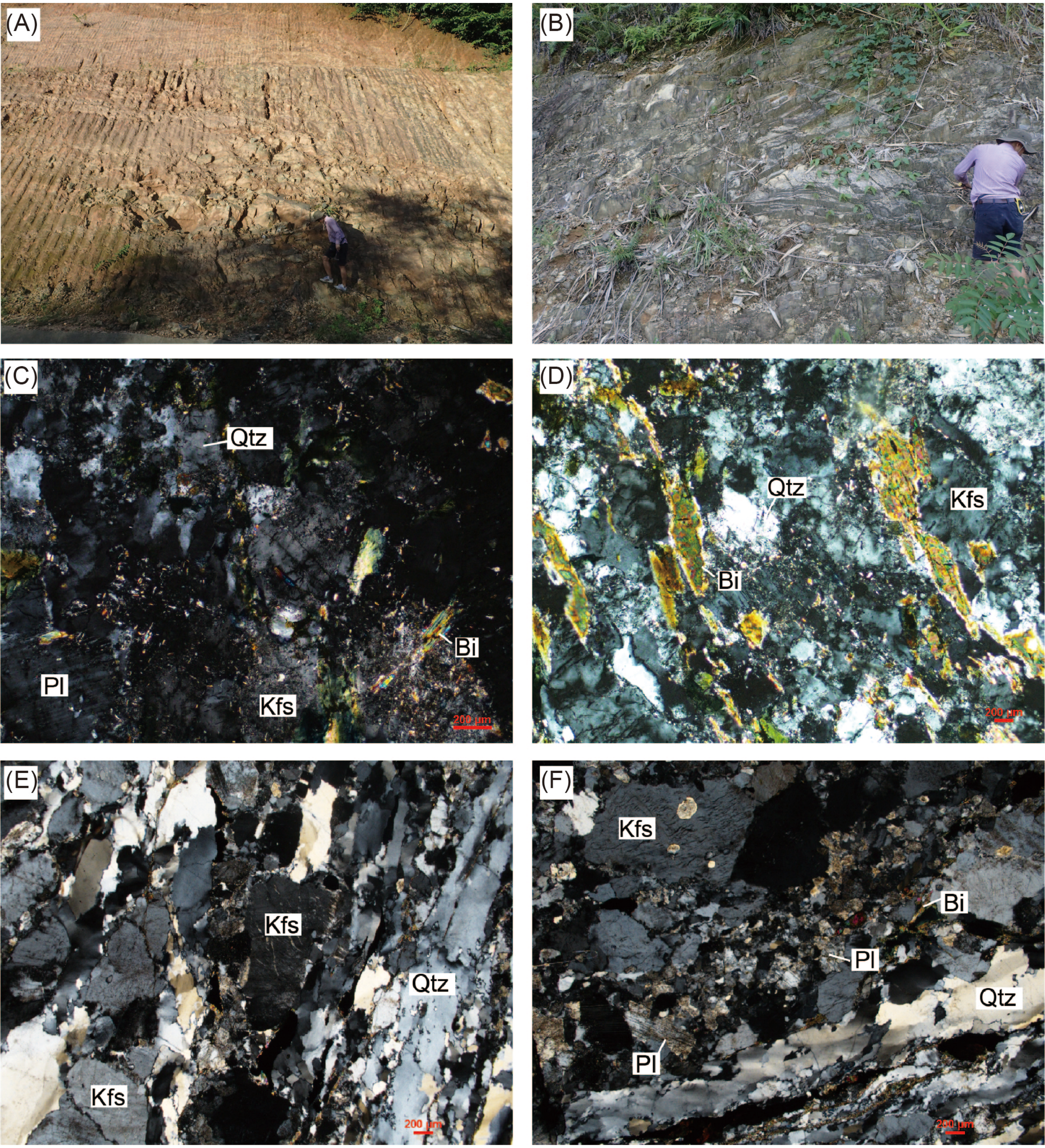
(A)
(B)
(C)
Qtz
Bi
Pl
Kfs
200 μm
(D)
Qtz
Kfs
Bi
200 μm
(E)
Kfs
Qtz
Kfs
200 μm
(F)
Kfs
Bi
Pl
Qtz
Pl
200 μm

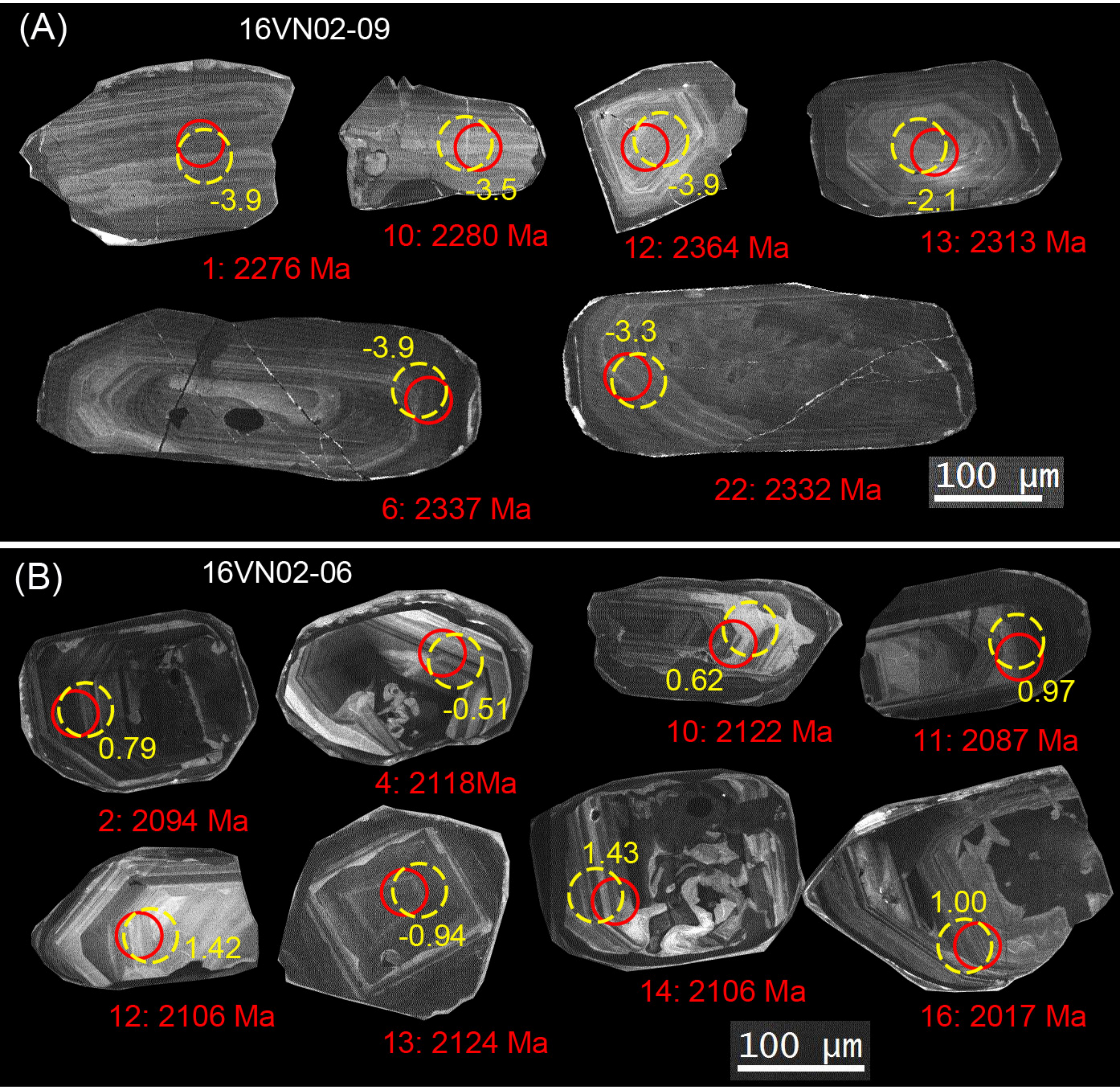

(A)
16VN02-09
-3.9
1: 2276 Ma
-3.5
10: 2280 Ma
-3.9
12: 2364 Ma
-2.1
13: 2313 Ma
-3.9
6: 2337 Ma
-3.3
22: 2332 Ma
100 μm
(B)
16VN02-06
0.79
2: 2094 Ma
-0.51
4: 2118Ma
0.62
10: 2122 Ma
0.97
11: 2087 Ma
1.42
12: 2106 Ma
-0.94
13: 2124 Ma
1.43
14: 2106 Ma
1.00
16: 2017 Ma
100 μm

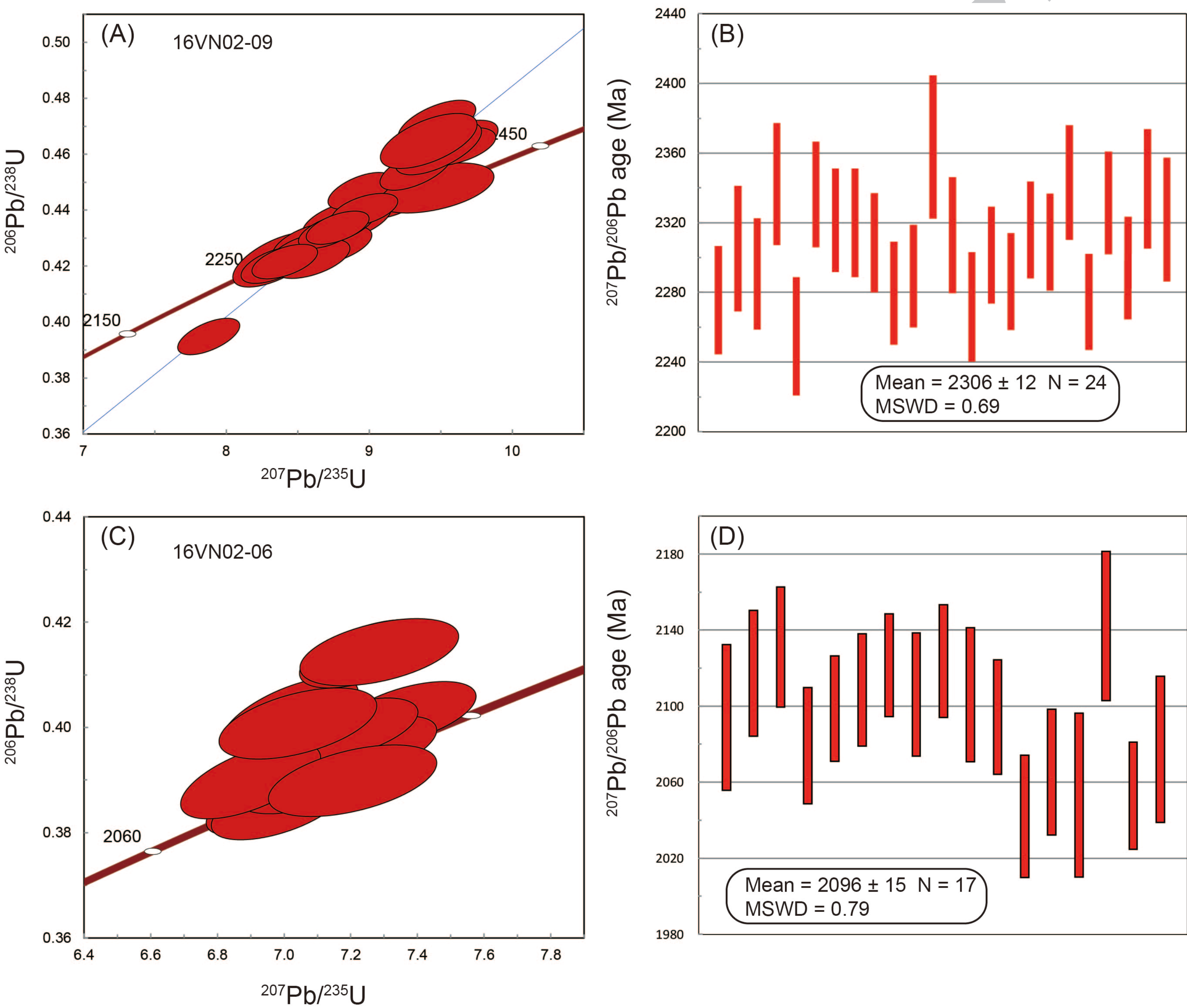
(A)
16VN02-09
2150
2250
2450
0.50
0.48
0.46
0.44
0.42
0.40
0.38
0.36
7
8
9
10
206Pb/238U
207Pb/235U
(B)
2440
2400
2360
2320
2280
2240
2200
207Pb/206Pb age (Ma)
Mean = 2306 ± 12 N = 24
MSWD = 0.69
(C)
16VN02-06
2060
0.44
0.42
0.40
0.38
0.36
6.4
6.6
6.8
7.0
7.2
7.4
7.6
7.8
206Pb/238U
207Pb/235U
(D)
2180
2140
2100
2060
2020
1980
207Pb/206Pb age (Ma)
Mean = 2096 ± 15 N = 17
MSWD = 0.79

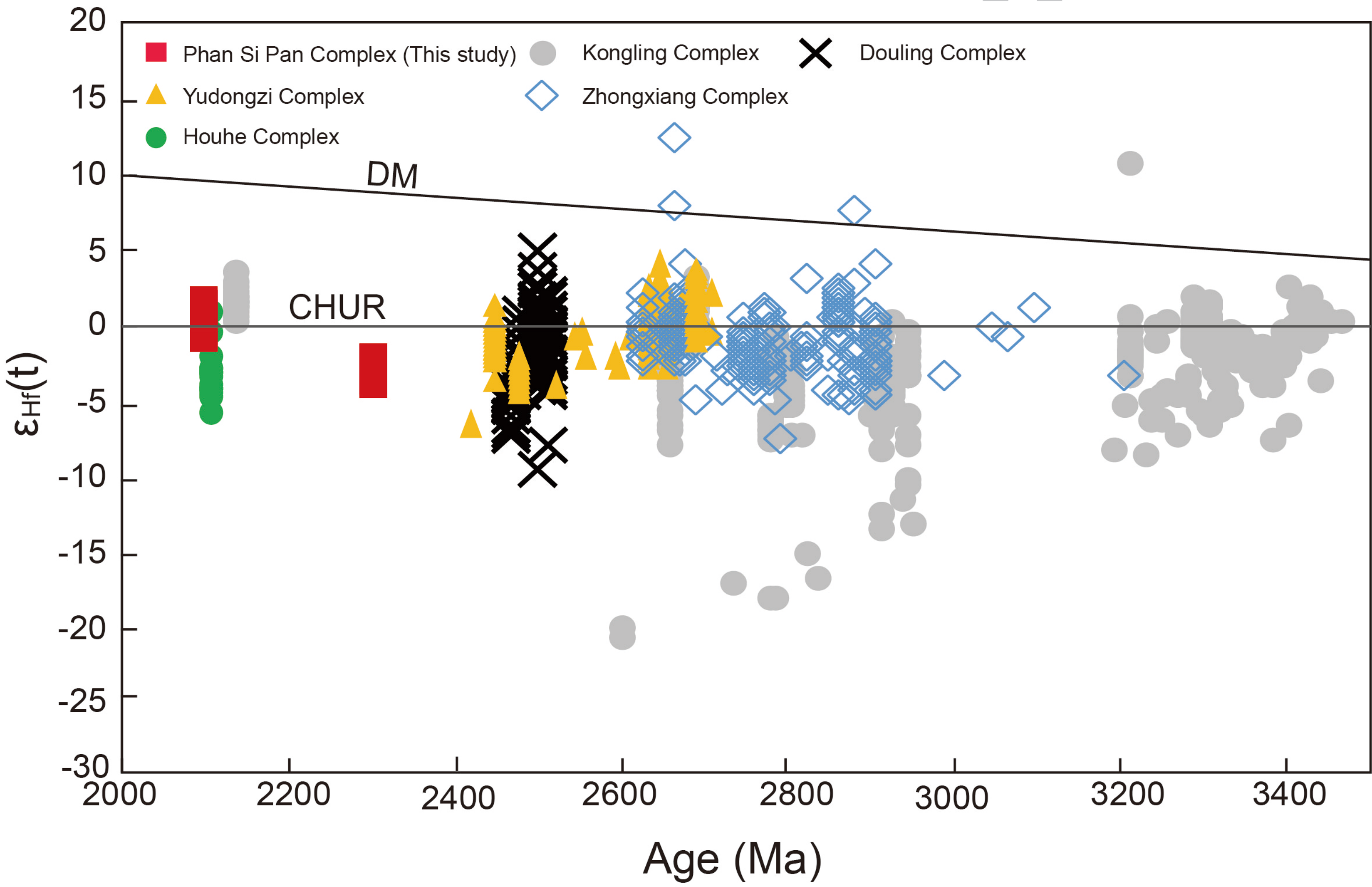
Phan Si Pan Complex (This study)
Kongling Complex
Douling Complex
Yudongzi Complex
Zhongxiang Complex
Houhe Complex
DM
CHUR
20
15
10
5
0
-5
-10
-15
-20
-25
-30
εHf(t)
2000
2200
2400
2600
2800
3000
3200
3400
Age (Ma)

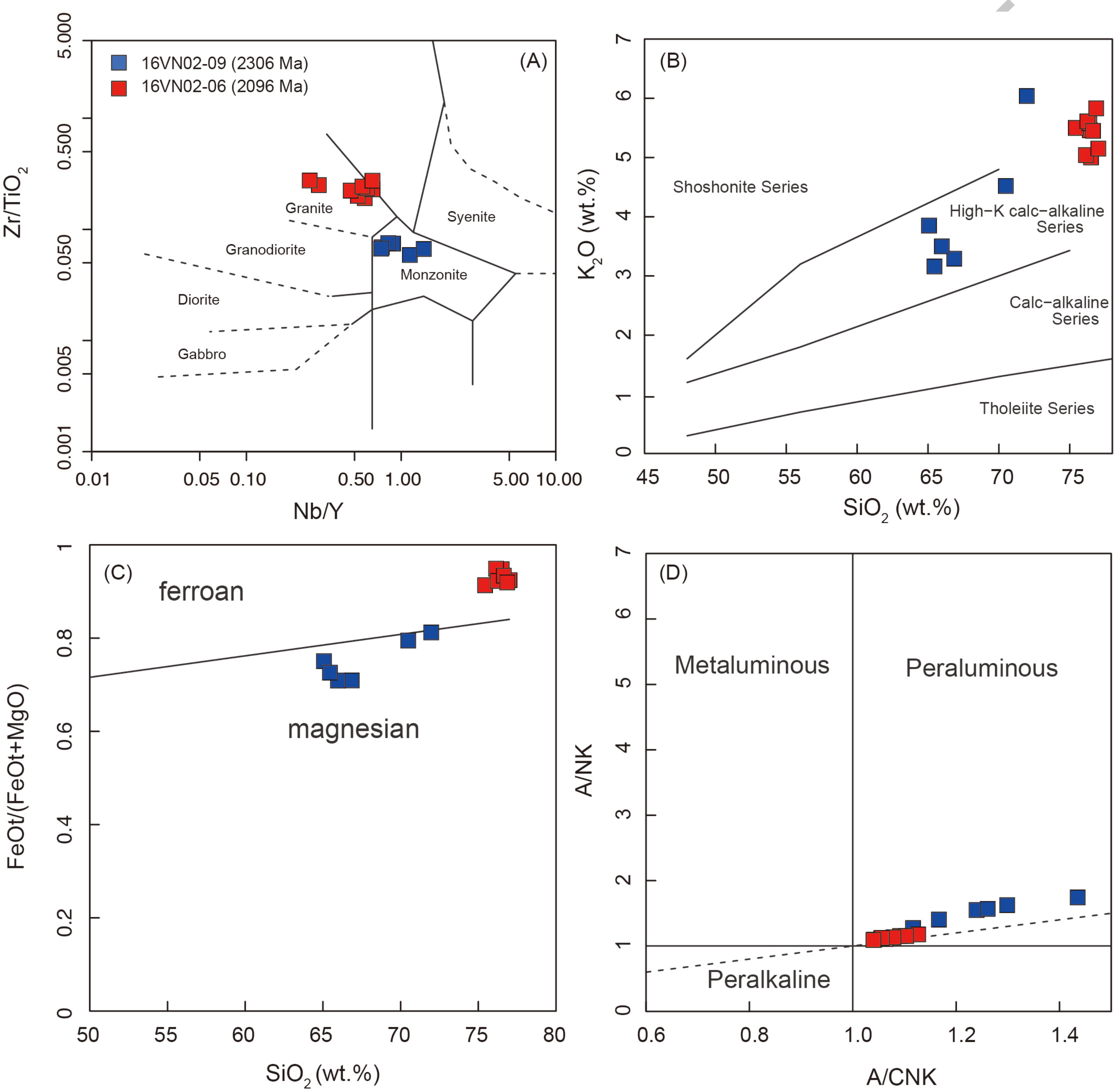
16VN02-09 (2306 Ma)
16VN02-06 (2096 Ma)
(A)
Zr/TiO2
Nb/Y
Granite
Syenite
Granodiorite
Monzonite
Diorite
Gabbro
(B)
K2O (wt.%)
SiO2 (wt.%)
Shoshonite Series
High−K calc−alkaline Series
Calc−alkaline Series
Tholeiite Series
(C)
ferroan
magnesian
FeOt/(FeOt+MgO)
SiO2 (wt.%)
(D)
Metaluminous
Peraluminous
Peralkaline
A/NK
A/CNK

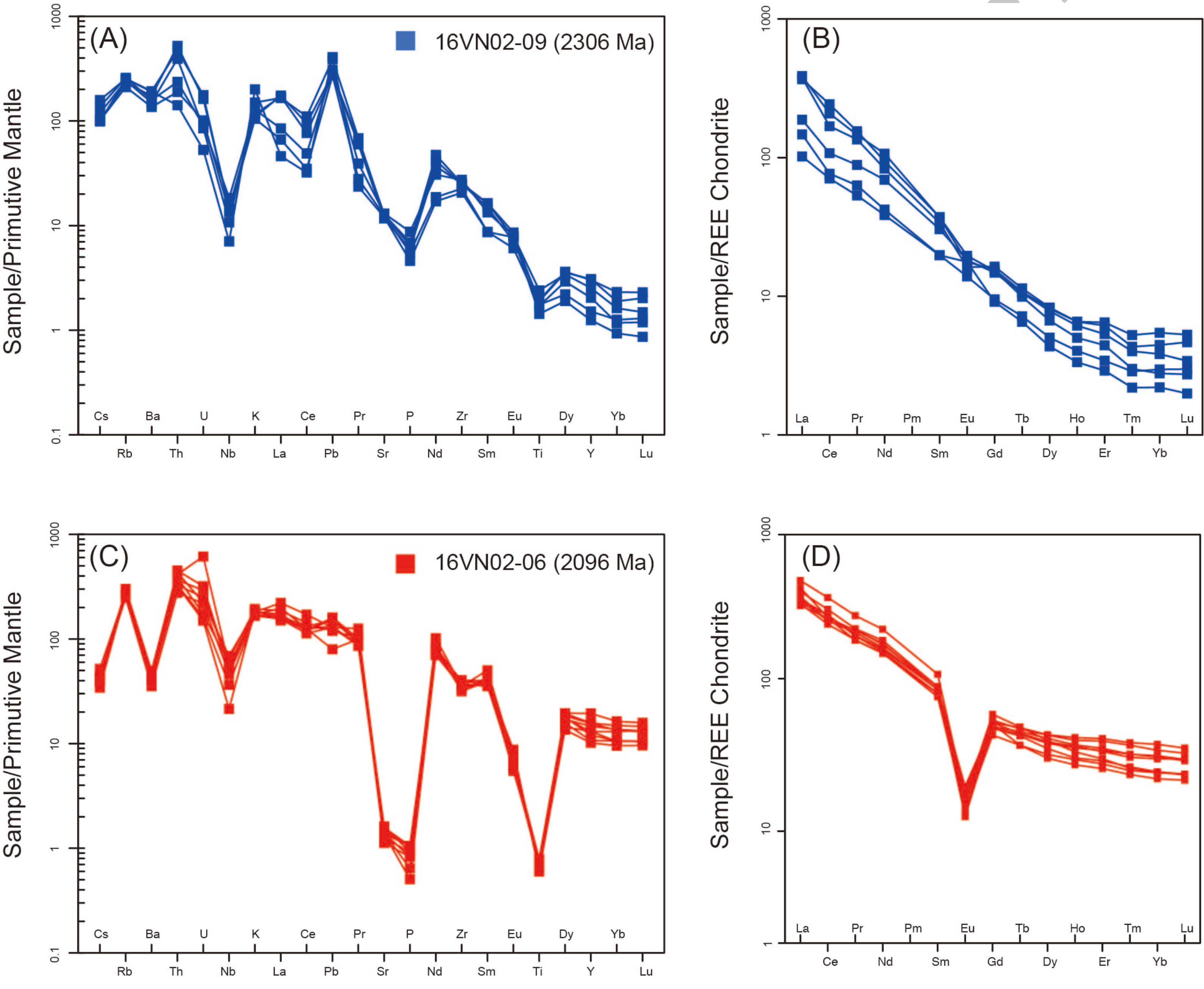
(A)
16VN02-09 (2306 Ma)
Sample/Primitive Mantle
1000
100
10
1
0.1
Cs
Rb
Ba
Th
U
Nb
K
La
Ce
Pb
Pr
Sr
P
Nd
Zr
Sm
Eu
Ti
Dy
Y
Yb
Lu
(B)
Sample/REE Chondrite
1000
100
10
1
La
Ce
Pr
Nd
Pm
Sm
Eu
Gd
Tb
Dy
Ho
Er
Tm
Yb
Lu
(C)
16VN02-06 (2096 Ma)
Sample/Primitive Mantle
(D)
Sample/REE Chondrite

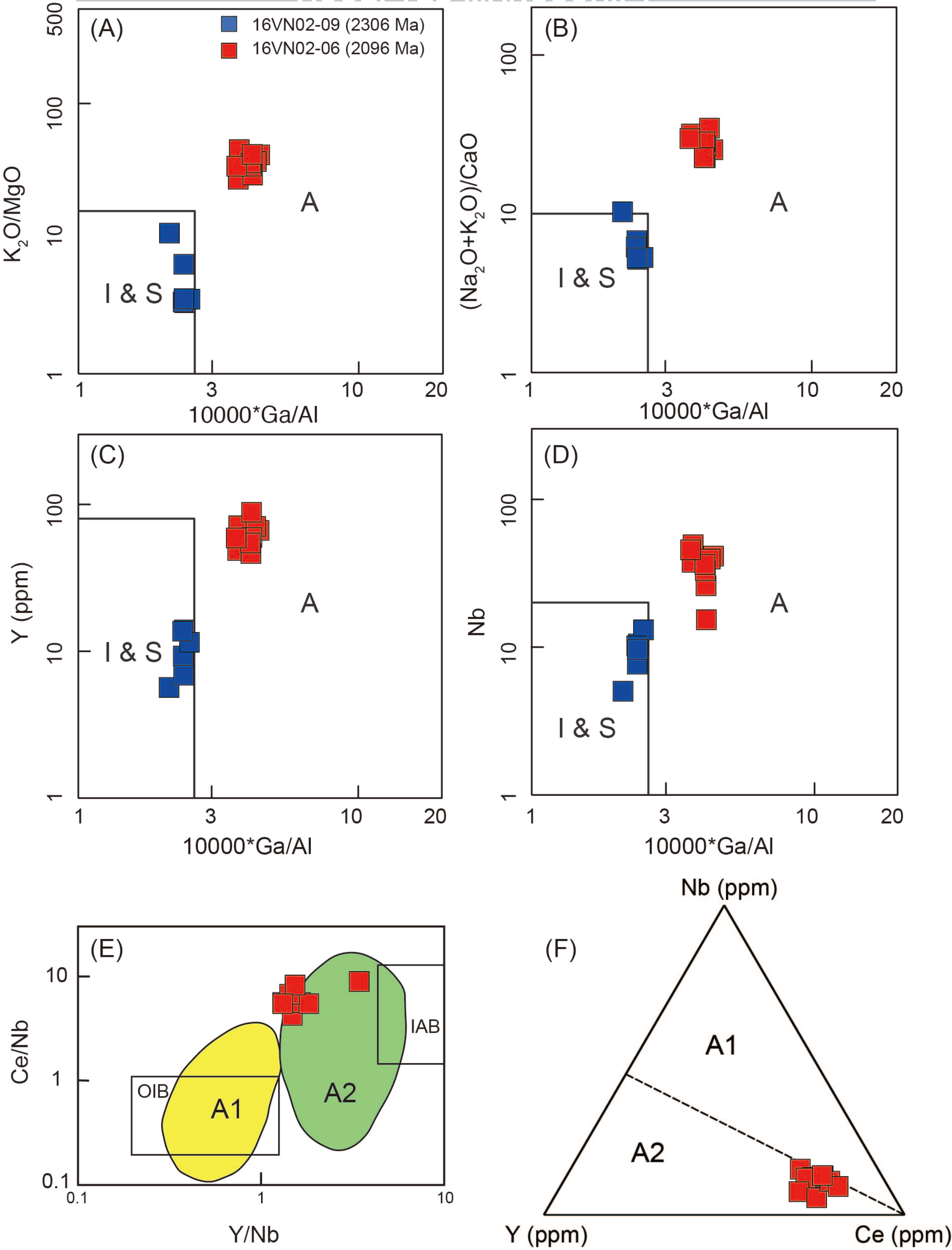
(A)
16VN02-09 (2306 Ma)
16VN02-06 (2096 Ma)
K2O/MgO
10000*Ga/Al
A
I & S
(B)
(Na2O+K2O)/CaO
10000*Ga/Al
A
I & S
(C)
Y (ppm)
10000*Ga/Al
A
I & S
(D)
Nb
10000*Ga/Al
A
I & S
(E)
Ce/Nb
Y/Nb
OIB
A1
A2
IAB
(F)
Nb (ppm)
Y (ppm)
Ce (ppm)
A1
A2

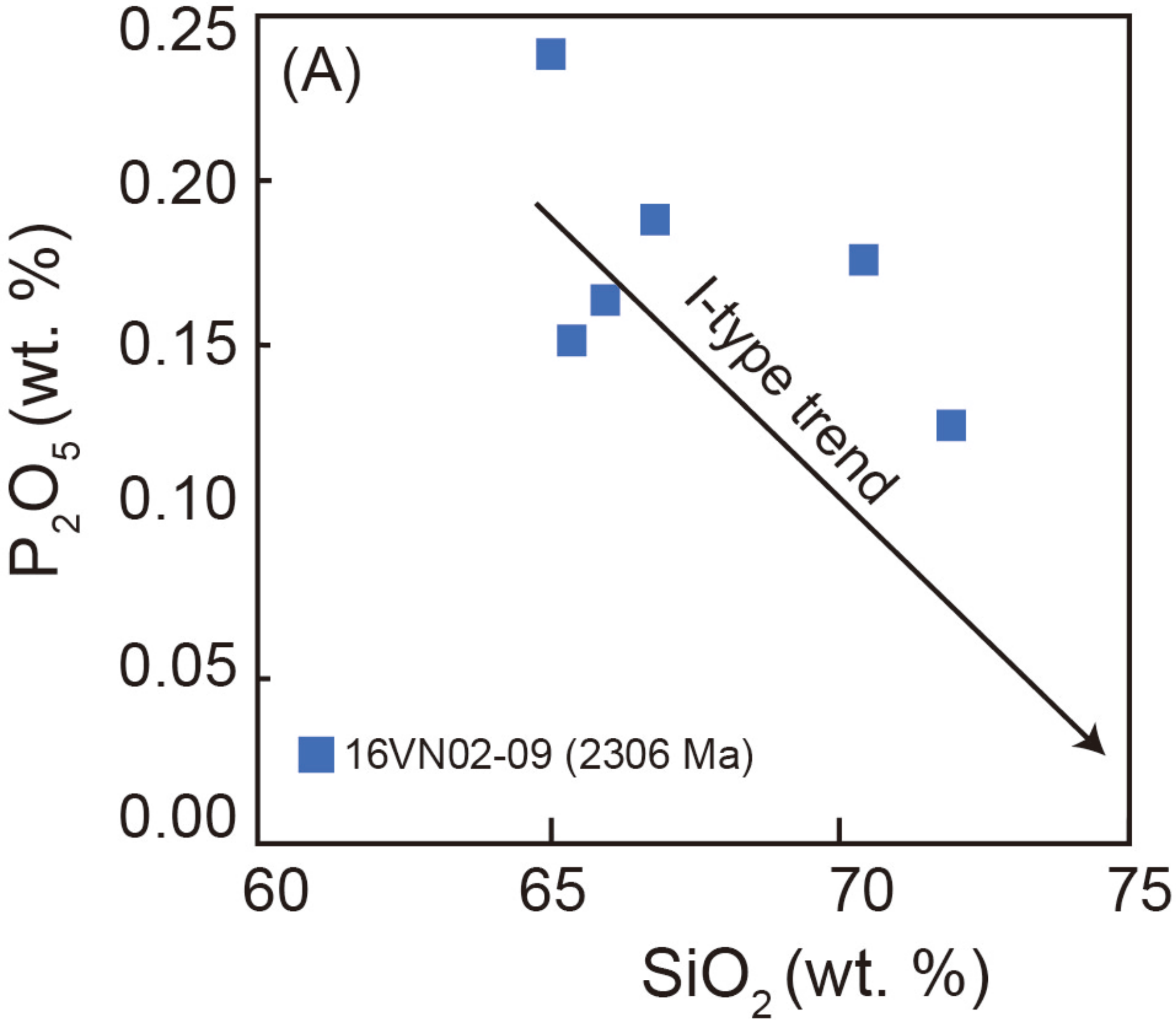
(A)
I-type trend
16VN02-09 (2306 Ma)
0.25
0.20
0.15
0.10
0.05
0.00
60
65
70
75
P_2O_5 (wt. %)
SiO_2 (wt. %)

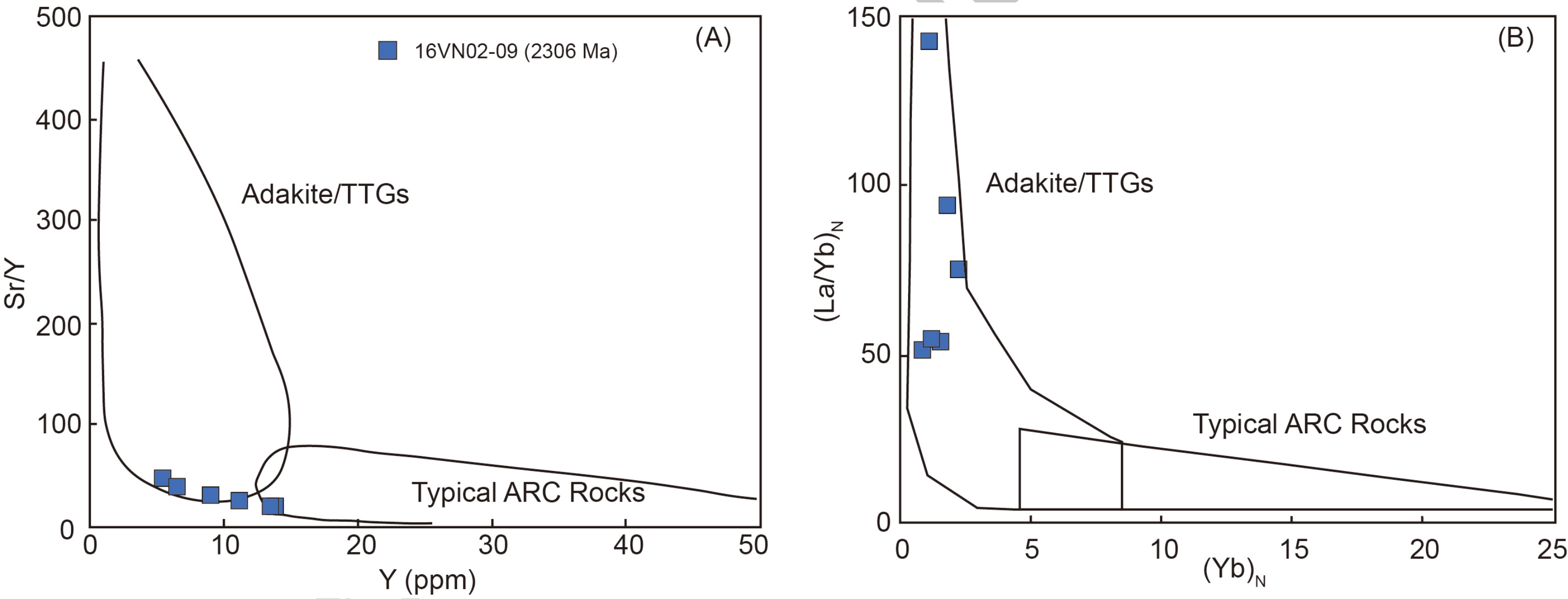

500
400
300
200
100
0
Sr/Y
0
10
20
30
40
50
Y (ppm)
16VN02-09 (2306 Ma)
(A)
Adakite/TTGs
Typical ARC Rocks
150
100
50
0
(La/Yb)N
0
5
10
15
20
25
(Yb)N
(B)
Adakite/TTGs
Typical ARC Rocks

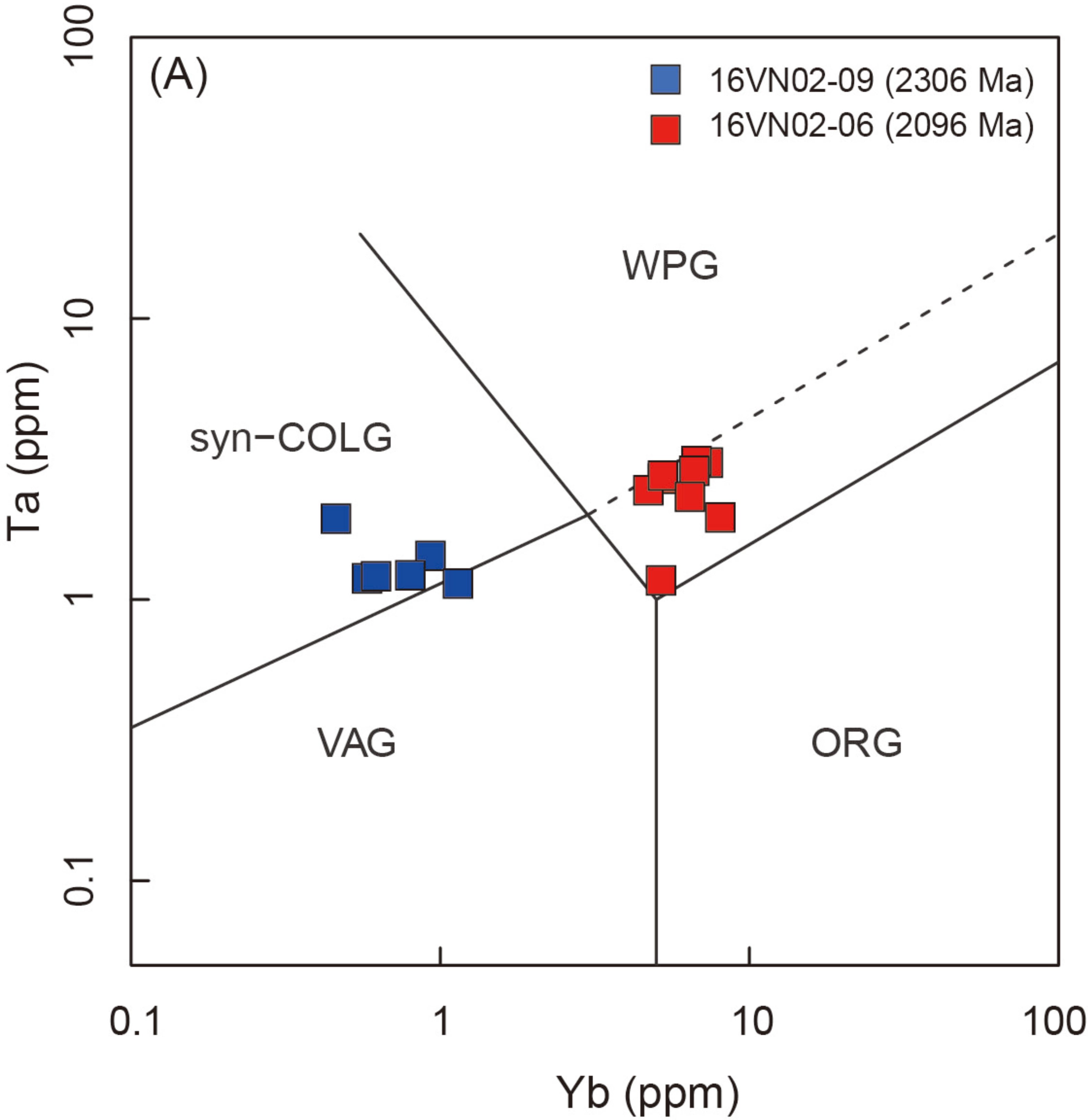

(A)
16VN02-09 (2306 Ma)
16VN02-06 (2096 Ma)
WPG
syn−COLG
VAG
ORG
Ta (ppm)
Yb (ppm)
0.1
1
10
100

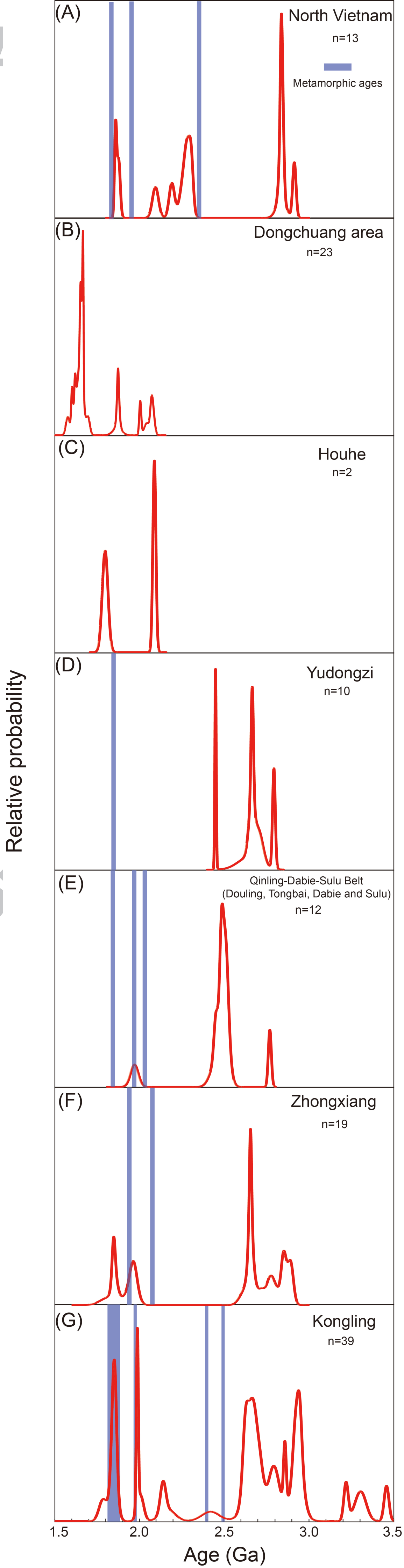

(A)
North Vietnam
n=13
Metamorphic ages
(B)
Dongchuang area
n=23
(C)
Houhe
n=2
(D)
Yudongzi
n=10
(E)
Qinling-Dabie-Sulu Belt
(Douling, Tongbai, Dabie and Sulu)
n=12
(F)
Zhongxiang
n=19
(G)
Kongling
n=39
Relative probability
1.5
2.0
2.5
3.0
3.5
Age (Ga)

Table 1. Compilation of ca. 2.3 Ga magmatic and tectonic events around the world. All ages are zircon U-Pb ages.

Geographic location and craton	*Unit name*	*Rock composition*	*Tectonic setting*	*Age (Ma)*	*εNd*	*εHf*	*Reference*
Canada							
Rae Craton	North Shore Plutons	Monzogranite	Syn- to post-collisional	2287~2326	-6.7, -1.5	-0.5 to -3.6	[1,2]
Rae Craton	North Shore Plutons	Tonalite	Syn- to post-collisional	2320 ± 44	n.a.	n.a.	[1]
Rae craton	Zemlak Domain	Granodiorite	Syntectonic	2316~2330	-5	n.a.	[3]
Asia							
Tarim Craton	Quanji Massif	Diorites	Extensional	2344~2370	-1.5, -1.2	-1.4 to 2.3	[4]
Tarim Craton	Quanji Massif	Granodiorites	Extensional	2337~2341	n.a.	-1.8 to 2.3	[4]
Tarim Craton	Quanji Massif	Quartz-diorite	Extensional	2392~2394	n.a.	0.4 to 7.6	[5]
Tarim Craton	Heluositan Group	Granite	Continental rift	2343~2410	-4.7 to -0.4		[6]
North China Craton	Taihua Complex	Granitic gneisses	Island arcs	2313~2363	-3.5 to 3.8	-7.2 to 2.3	[7]
North China Craton	Taihua Complex	Amphibolitic gneiss	Island arcs	2313 ± 11	4.2	0.4 to 1.2	[7]
North China Craton	Taihua Complex	Tronhjemitic gneiss	Island arcs	2316±14	-1	-7.3 to -0.4	[7]
North China Craton	Luliang Complex	Granitic gneisses	Arc-related	2375 ± 10	n.a.		[8]
North China Craton	Luliang Complex	Felsic gneiss	Continental arc	2291	n.a.	1.1 to 9.6	[9]
North China Craton	Luliang Complex	Meta-gabbro	Continental arc	2323±5	n.a.	-2.06 to 1.82	[10]
North China Craton	Hengshan Terrain	Granitic gneisses	Continental arc	2330~2359	n.a.	n.a.	[11]
Dharwar Craton	Dharwar giant dyke swarm	Mafic dyke	LIP/mantle-plume event	2365~2369	n.a.	n.a.	[12,13]
Yangtze Block	Dongchuan Area	Ignimbrite	n.a.	2285 ± 11	n.a.	n.a.	[14]
Yangtze Block	Dongchuan Area	Felsic tuff	n.a.	2299 ± 14	n.a.	n.a.	[15]
Yangtze Block	North Vietnam	Quartz monzonites	Syn-collision	2303 ± 12			
Africa							
Zimbabwe Craton	Chimbadzi Hill Intrusion	Mafic-ultramafic	Prmitive mantle-derived melt	2262 ± 2	n.a.	n.a.	[16]
Congo Craton	Ntem Complex	Two-pyroxene syenite	Extension or even rifting	2321±1	-7.5 to-5.8	n.a.	[17]
Congo Craton	Ntem Complex	Clinopyroxene syenite	Prmitive mantle-derived melt	2349±1	-7.5 to-6.2	n.a.	[17]
South America							
São Francisco Craton	Mineiro belt	Orthogneiss	Island arcs	2305~2351	-9.2 to 6.2	n.a.	[18]
São Francisco Craton	Mineiro belt	Amphibolite	Island arcs	2317 ± 16	0.4 to 7.1	n.a.	[18]
São Francisco Craton	Lagoa Dourada suite	Tonalite	Intra-oceanic arc	2349 ± 4	1.0 to 2.1	n.a.	[19]
São Francisco Craton	Lagoa Dourada suite	Trondhjemite	Intra-oceanic arc	2356 ± 3			[19]
Amazonian craton	Bacajá domain	Metandesite	Island arcs	2359 ± 2	-0.87 to 0.78	n.a.	[20]
Amazonian craton	Bacajá domain	Tonalitic gneiss	Island arcs	2356 ± 7	0.4 to 0.5	n.a.	[21]
Amazonian craton	Bacajá domain	Granodioritic gneiss	Island arcs	2358 ± 20	0.7 to 1.5	n.a.	[21]
Borborema Province	Me´dio Coreau´domain	Tonalitic gneiss	Island arcs	2288±2	0.5 to 1.9	n.a.	[22]
Europe							
North Atlantic Craton	West Greenland	Gabbroic dyke	LIP event	2365~2374	n.a.	n.a.	[23]
Karelian Craton	Lake Upper Kuito	Mafic dykes	LIP/rifting events	2309±3	0.5 to 0.8	n.a.	[24]
Fennoscandian Shield	West Troms Basement complex	Dyke swarm	LIP event	2403 ± 3	-1.5 to -1.8	n.a.	[25]

Data source: [1]: Hartlaub et al., (2007); [2]: Partin et al., (2014); [3]: Ashton et al., (2007); [4]: He et al., (2014); [5]: Gong et al., (2014); [6]: Zhang et al., (2007); [7] Diwu et al., (2014); [8]: Zhao et al., (2008); [9]: Santosh et al., (2015); [10]: Yuan et al., (2017); [11]: Kröner et al., (2005); [12]:

Kumar et al., (2012); [13]: French et al., (2010); [14]: Zhu et al., (2011); [15]: Zhou et al., (2012); [16]: Manyeruke et al., (2004); [17]: Tchameni et al., (2001); [18]: Teixeira et al., (2015); [19]: Seixas et al., (2012); [20]: Macambira et al., (2009); [21]: Dos Santos et al., (2009); [22]: Dos Santos et al., (2008); [23]: Nisson et al., (2013); [24]:Stepanova et al., (2015); [25]: Kullerud et al., (2006).

- Early Paleoproterozoic magmatism were reported in Phan Si Pan Complex in North Vietnam of the Yangtze Block.
- The ca. 2.3 Ga quartz monazite formed at a collision-related crustal thickening event.
- The ca. 2.1 Ga A-type gneissic granite formed within an extensional tectonic setting.
- The Phan Si Pan Complex was an independent terrane separated from other parts of the Yangtze Block during the early Paleoproterozoic.
- The Yangtze Block was linked to northwestern Laurentia in the Pre-Nuna supercontinent.